iScience

CellPress
OPEN ACCESS

Review

Stereolithography apparatus and digital light processing-based 3D bioprinting for tissue fabrication

Wanlu Li,[1,3] Mian Wang,[1,3] Huiling Ma,[1] Fabiola A. Chapa-Villarreal,[1] Anderson Oliveira Lobo,[2,*] and Yu Shrike Zhang[1,*]

SUMMARY

Three-dimensional (3D) bioprinting has emerged as a class of promising techniques in biomedical research for a wide range of related applications. Specifically, stereolithography apparatus (SLA) and digital light processing (DLP)-based vat-polymerization techniques are highly effective methods of bioprinting, which can be used to produce high-resolution and architecturally sophisticated structures. Our review aims to provide an overview of SLA- and DLP-based 3D bioprinting strategies, starting from factors that affect these bioprinting processes. In addition, we summarize the advances in bioinks used in SLA and DLP, including naturally derived and synthetic bioinks. Finally, the biomedical applications of both SLA- and DLP-based bioprinting are discussed, primarily centered on regenerative medicine and tissue modeling engineering.

INTRODUCTION

Three-dimensional (3D) bioprinting accurately patterns biochemicals, biological materials, and/or following computer designs to recapitulate the native tissues, aiming to provide cellular, structural, and environmental cues facilitating biomedical applications.[1,2] Although the emergences of the few pioneering bioprinting demonstrations were quite close to each other, extrusion bioprinting was arguably the first modality showcased by Mülhaupt et al. (2002),[3] followed by inkjet bioprinting (2003)[4–6] and stereolithography apparatus (SLA)-based bioprinting (2004),[7,8] both by Boland's team.

Now through two decades of development, primary bioprinting approaches have emerged to particularly focus on the extrusion-based technique driven by the mechanical or pneumatic force.[9] Extrusion bioprinting utilizes the deposition of filaments of cell-laden bioinks, and builds the designed constructs driven in a layer-by-layer manner. However, the limited resolution (>100 μm) of the extrusion approach as well as its generally slow fabrication process impede its capacity to recapitulate the sophisticated tissue microenvironments.[10,11] On the other hand, vat-polymerization (VP) methods, including the aforementioned SLA and the more recently popularized digital light processing (DLP),[12,13] have attracted increasing attention in tissue biofabrication. VP-based bioprinting harnesses high-resolution photopolymerization for the creation of 3D constructs when exposing the liquid bioink to patterned light.[14,15] Although SLA and DLP are both layer-by-layer fabrication approaches, the latter uses projected planner light patterns and hence, faster than SLA that relies on raster scans.[16]

VP-based bioprinting has been extensively investigated for fabricating *in vitro* microtissue models for drug discovery and functional tissues for regenerative medicine.[17,18] Further development of biomaterials enables successful incorporation of living cells and bioactive agents into printable bioinks specifically designed for VP applications.[19–21] Herein, we first provide a brief overview on the SLA and DLP bioprinting principles. State-of-the-art bioinks used for building tissue constructs are subsequently reviewed. Finally, we highlight the biomedical applications on tissue model engineering and regenerative medicine of VP-based bioprinting. At the end, a perspective on the outlook of these technologies is presented. Of note, while we mostly focus on bioprinting (i.e., printing in the presence of living cells), certain examples that have reported on post-printing cell seeding are also included due to their potential for adapting to bioprinting.

SLA

SLA is a conventional VP process, which has been demonstrated as one of the most common 3D printing technologies, exhibiting exceptional precision to spatially fabricate 3D constructs. The working mechanism

[1]Division of Engineering in Medicine, Department of Medicine, Brigham and Women's Hospital, Harvard Medical School, Cambridge, MA 02139, USA

[2]Interdisciplinary Laboratory for Advanced Materials (LIMAV), Materials Science and Engineering Graduate Program (PPGCM), Federal University of Piauí (UFPI), Teresina, PI 64049-550, Brazil

[3]These authors contributed equally

*Correspondence: lobo@ufpi.edu.br (A.O.L.), yszhang@research.bwh.harvard.edu (Y.S.Z.)

https://doi.org/10.1016/j.isci.2023.106039

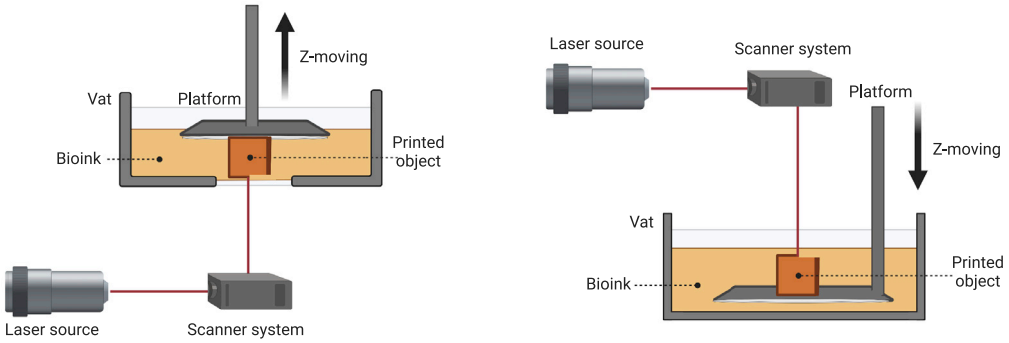

Figure 1. Schematic of SLA-based bioprinting

Laser provides light for the photopolymerization of bioink in vat through a computer-controlled moving laser beam. When a layer is completely bioprinted via point-by-point curing, the build platform will lift up (left) or move down (right) in the z-direction until the bioprinted object is finished line-by-line and layer-by-layer.

of SLA-based 3D bioprinting is no different from 3D printing, and is dependent on a computer-controlled laser beam to cure a liquid photocrosslinkable bioink (Figure 1).[22,23] Upon exposure to the raster-scanning laser, the liquid bioink can be cured onto a vertical-driven (z-direction) build platform. After photocrosslinking of the first layer, the platform is moved away from the printing position to refill fresh liquid bioink for photocuring of the second layer. As such, with repetition of this iteration, 3D-bioprinted constructs with specific characteristics can be eventually obtained.[24] When the entire process is finished, the bioprinted sample may require extra post-polymerization processing, such as heating or additional photocuring.[25,26]

One of the main advantages of SLA is that the printing resolution, which aside from dependence on printing speed, direction, and volume, can be enhanced by lowering the spot size of the laser, reaching up to 10 μm[24,27,28] Even though most protocols for SLA include non-water-soluble photoinitiators, which are typically inappropriate for bioprinting, and that ultraviolet (UV) light is not the best option for cells, some reports have successfully bioprinted cells using properly engineered bioinks.[7,29] Chan et al. encapsulated NIH/3T3 cells, a mouse fibroblast cell line, into poly(ethylene glycol)-diacrylate (PEGDA, molecular weight, M_w = 700 to 10,000 Da) using an SLA method.[30] From the results of 3-(4,5-dimethylthiazol-2-yl)-5-(3-carboxymethoxyphenyl)-2-(4-sulfophenyl)-2H-tetrazolium (MTS) assay, they demonstrated that the cells exhibited long-term metabolic activities up to 14 days of culture by increasing the Mw of PEGDA. Meanwhile, adding the Arg-Gly-Asp-Ser (RGDS) peptide was able to enhance the cell viability compared to PEGDA of the same Mw but without RGDS. However, the study only evaluated the metabolic activities of NIH/3T3 fibroblasts. More investigations are needed to assess additional cellular functions, not only for cell lines, but also for primary cells and stem cells that are likely more important cell sources in tissue regeneration and organ modeling.

DLP

DLP is another type of VP printing that is quite similar to SLA, but the major difference between the two systems is the light patterning style. SLA is associated with raster laser scanning, whereas DLP is based on the two-dimensional (2D) photopolymerization using a digital mirror device (DMD) or a liquid crystal display (LCD) projection system.[31] DMD is an array containing up to several millions of micromirrors that switches positions between 'on' and 'off', and only reflects the light in the 'on'-state mirrors.[14,32] The bioink is photocrosslinked by projecting the light from the aforementioned digital mask with a complete 2D layer in individual light exposure.[33] Therefore, a faster build time in general, is provided by DLP compared to the SLA approach, the former of which only depends on the height of the 3D constructs in the z-direction.[34]

DLP bioprinting can further be classified into two sub-types according to the moving directions in the z axis: top-down and bottom-up (Figure 2).[18] In the top-down configuration, the build platform is submerged and covered with the bioink, and moved further down to the next photopolymerization layer.[35] This method benefits the bioprinting of soft materials because it lacks the requirement of the pulling-up force of hydrogels. Nevertheless, it might generate irregular layers as the filling bioink cannot settle evenly on the surface owing to surface tension. Also, submerging bioprinted structures in liquid bioink during the printing process demands a larger bioink volume to keep the bioink refill to the top surface. On the other hand, the

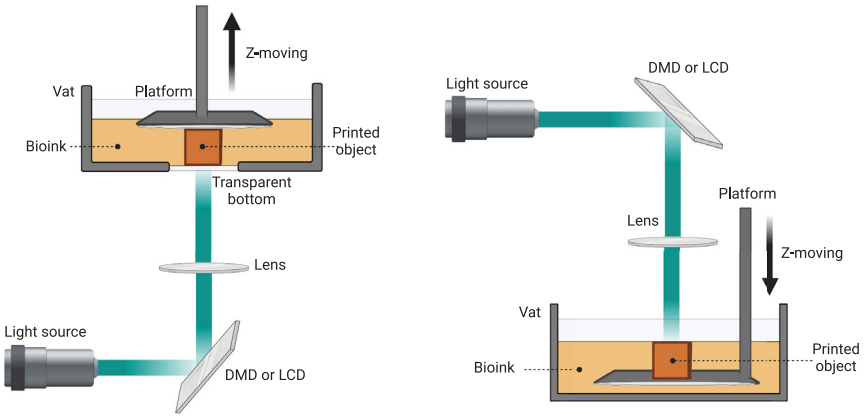

Figure 2. Illustrations of DLP-based bioprinting systems (bottom-up (left), top-down (right))

The light pattern projected by DMD or LCD is focused by lens to reach the vat bottom (bottom-up) or liquid surface (top-down). The bioink held in the vat is photocrosslinked by a 2D image at a single printing time, followed by the repeated process of lifting up (bottom-up) or moving down (top-down) of the build platform until the entire object is bioprinted layer-by-layer.

bottom-up DLP bioprinter consists of the platform suspended over the bioink vat and moved up after each layer of photopolymerization. For this type of bioprinting, a transparent anti-adherent bottom, such as a thin film made by polydimethylsiloxane (PDMS) or Teflon membrane, is required.[35,36] The bottom-up configuration shows numerous advantages in bioink-saving because the construction height does not depend on the vat depth, and continuous bioprinting can be achieved to obtain 3D constructs with flat sidewalls.[37] As a result, the bottom-up DLP system serves as a widely used DLP bioprinting technique. It is extensively applied in various biomedical fields, providing a novel strategy to fabricate 3D structures with sophisticated geometries and good surface qualities in a time-saving and bioink-saving manner.

Although SLA/DLP-based bioprinting endows the benefits of high resolution and fast speed, these techniques suffer from some limitations because of the requisites of bioink properties for printability. For example, the bioink must be readily photocrosslinked through light-irradiation and must possess relatively low viscosity, so that the uncured bioink continuously interfaces with the cured layers beforehand. In addition, SLA/DLP-based 3D bioprinting has been largely restricted to building planar but not truly volumetric structures; it is oftentimes difficult to address the issue in bioprinting with ultra-soft bioinks because the force exerted onto the fabricated constructs can result in deformation or even collapse during the layer-by-layer bioprinting process.

FACTORS AFFECTING SLA/DLP-BASED BIOPRINTING

Photopolymerization, also known as photocuring or photocrosslinking, is the main principle underlying the SLA/DLP-based bioprinting. By exciting a photoinitiator via appropriate light, free radicals are generated to promote the chain growth of monomers or oligomers.[38] In SLA/DLP-based bioprinting, optimizing the laser scanning setups of SLA methods and projection systems in DLP approaches, the selection of the suitable light source as well as the photoinitiator are crucial to ensuring effective printing, allied to the addition of the photoabsorber that assists proper resolution-achievement. This section will discuss these factors influencing the processes associated with SLA/DLP-based 3D bioprinting. Moreover, another element, the mechanical properties of the crosslinked hydrogels, cannot be overlooked when SLA/DLP-based bioprinting is applied to fabricate tissue-specific mimics. Overall, the polymerization efficiency, printing resolution, and accuracy are critical indexes to evaluate the 3D bioprinting results.

Laser/projection system

The lateral resolution of SLA or DLP bioprinting is limited by the laser size or pixel size provided by the DMD.[39] In the SLA method, a laser beam (minimum ~1 μm) is focused through a high-magnification objective lens to induce polymerization of the bioinks,[40] fabricating structures at a submicron resolution. For the DLP system, reducing the pixel size of DMD (an increase of the pixel numbers in the same

projection area) benefits to the finer light spot projected. In addition, the setup of a DLP bioprinter also involves the magnifications/demagnifications of projection area onto bioinks by placing lenses. The projection area then gets larger/smaller, accompanied by the pixel size increase/decrease, which leads to a trade-off between the projection area (printing scale) and pixel size (xy resolution). The home theater projector with a display resolution of 1920 × 1080 pixels,[41] and the Optical Engine (1280 × 800 pixels or 1920 × 1080 pixels) based on DMD chips have been widely used in the DLP-base 3D bioprinting to achieve the finest xy resolution of 10 μm and the projection area 96 × 54 mm.[42] Applying 4K (3840 × 2160 pixels) DMD chips may provide the possibilities to obtain resolutions while maintaining a large building area.[43] Moreover, the light wavelength will also influence the optical resolution, where shorter wavelengths deliver better optical resolution.[44]

Photoinitiator

Photoinitiator is the key element in photopolymerization because it determines the efficiency of polymerization, resulting in the various printing times and resolutions in the SLA/DLP-based method. Photoinitiator is commonly composed of the photosensitive molecule with a relatively high molar extinction coefficient. Once excited by light, it generates free radicals or cations to cleavage the covalent bonds presented in functional groups, triggering polymerization.[38]

Depending on the chemical structure of the photoinitiator, the irradiation requires the use of light with a specific wavelength and intensity that ensure the desirable polymerization rate and efficiency.[45] Therefore, the first consideration in choosing an appropriate photoinitiator is determining the light wavelength applied in the printing procedure. The most common UV- or near-UV-sensitive photoinitiator systems employed in SLA/DLP-based bioprinting are 1-[4-(2-hydroxyethoxy)-phenyl]-2-hydroxy-2-methyl-1-propane-1-one (Irgacure 2959) and lithium phenyl-2,4,6-trimethylbenzoylphosphinate (LAP).[46] LAP possesses a much better molar absorptivity ($\varepsilon \approx 200 M^{-1}cm^{-1}$) than Irgacure 2959 ($\varepsilon \approx 10 M^{-1}cm^{-1}$), contributing to more efficient photoinitiation and can be used at lower concentrations. However, there is a concern when applying UV irradiation to bioinks encapsulating cells. Although it has been demonstrated that the low dose of UV (365 nm)-exposure shows no influence on the apoptosis and proliferation of NIH/3T3 fibroblasts and human mesenchymal stem cells (MSCs),[30]further studies on more cell types and other functional cellular activities are needed to fully conclude the cytocompatibility of UV wavelengths in bioprinting.

More recently, visible-light photoinitiators have attracted increasing attention because of their good biocompatibility and low phototoxicity. Eosin Y can be activated by the wavelengths between 490 and 650 nm ($\varepsilon \approx 100{,}000 M^{-1}cm^{-1}$), but the generation of free radicals requires both coinitiator (triethanolamine (TEOA)) and comonomer (1-vinyl-2 pyrrolidinone (NVP)).[47] Of note, LAP, a UV-sensitive photoinitiator discussed above, can also be utilized as a photoinitiator under a 405-nm blue light source. However, the limited molar absorptivity of LAP in this visible light range ($\varepsilon \approx 30 M^{-1}cm^{-1}$) leads to high concentrations to fabricate hydrogels. Another emerging visible-light initiating system, tris(2,2-bipyridyl)dichloro-ruthenium(II) hexahydrate/sodium persulfate (Ru/SPS), has shown promising results in SLA/DLP-based bioprinting. The excited Ru^{2+} is oxidized into Ru^{3+} and provides electrons to SPS at a high molar absorptivity ($\varepsilon \approx 14{,}600 M^{-1}cm^{-1}$). SPS then divides into sulfate anions and sulfate radicals for photocrosslinking by propagating of functional groups, including methacryloyl groups. In addition, the oxidized Ru^{3+} can further oxidize aromatic residues, such as tyrosine. As a result, the oxidized tyrosine groups are further converted into tyrosyl free radicals, and then form covalent di-tyrosine bonds with the other tyrosine moieties.[48–50] Indeed, it has been demonstrated that the Ru/SPS system could be applied to facilitate crosslinking of bioinks composed of or containing tyrosine-carrying proteins (e.g., decellularized extracellular matrix (dECM)).[49]

Photoabsorber

In the SLA/DLP-based bioprinting method, the lateral resolution is defined by the laser beam spot diameter (SLA) or the size of pixel being projected (DLP) onto the printing area, whereas the axial resolution is influenced by the movement resolution of the vertical build platform.[51] Moreover, the light can penetrate some distance into the bioink and decay exponentially in the propagation direction. Thus, the penetration depth of light also plays a pivotal role in determining axial resolution.

More specifically, the cure depth, also recognized as the light-penetration depth, is defined as the depth to which a 3D construct is photopolymerized to influence the vertical resolution and printing time of

SLA/DLP-based 3D printing.[18] When the cure depth is higher than the selected printing layer thickness, the out-of-focus plane will be over-crosslinked, leading to the inaccuracy of printing in the axial direction. To improve the axial resolution and adjust the desired printing thickness, light-absorbing additives, often known as photoabsorbers, are added for the absorption of excess crosslinking light. By incorporating photoabsorbers, the cure depth can be effectively decreased and tightly controlled.[52]

The most wildly used UV-absorbers are benzotriazole-derivatives, brilliant blue, and quinoline yellow.[53–55] For visible light, the general food dyes, such as tartrazine, curcumin (from turmeric), anthocyanin (from blueberries), acid red, and phenol red, have been applied in bioprinting, considering their known biocompatibility, low toxicity, as well as hydrophilic characteristic that enables for convenient elution after bioprinting.[56] Miller et al. selected tartrazine, a yellow food dye with an absorbance peak at 405 nm, in a 405-nm-light-enabled DLP system, to fabricate complex multivascular networks using PEGDA/gelatin methacryloyl (GelMA) bioinks.[42] They printed an alveolar model topology featuring perfusable open channels with 300-μm-diameter, which could not be achieved without the tartrazine additive. The authors also compared the results of other food dyes. Curcumin is more lipophilic than others, so it could not be efficiently removed and caused staining of the printed structures; whereas, anthocyanin with a peak absorbance far from the 405-nm printing light, required high concentrations to achieve targeted light-attenuation. Our recent study applied Ponceau 3R, a water-soluble food dye to print sophisticated 3D constructs using PEGDA, GelMA, or allylated gelatin (GelAGE)-based (bio)inks.[33] The absorbance peak of 507 nm enabled efficient light-absorption in our visible-light DLP 3D (bio)printing method.

Mechanical properties

The photocrosslinked hydrogel biomaterials for the DLP-based 3D bioprinting method need to be strong enough to support their structural fidelity against gravity, which is particularly true in the bottom-up configuration. The higher mechanical property oftentimes favors the printing procedure, but the obtained denser hydrogel constructs can negatively influence cell viability, spreading, and functionalities. A recent study developed a fluid-supported liquid interface polymerization (FLIP) 3D printing platform based on the buoyancy-assisted continuous DLP printing method.[57] It applied a support fluid immiscible with the inks to provide extra buoyant forces, allowing one to produce hydrogel constructs with stiffness values from approximately 7 kPa to more than 4 MPa. The buoyancy-assisted approach overcame the gravity requisitions in DLP-based 3D printing, enabling to print complex geometries with soft biomaterials. Besides the printing method modification, advances in bioink development also provide potential in DLP bioprinting of soft tissues. By modifying the GelMA concentration, the degree of substitution, and the photocrosslinking time, Sun et al. successfully controlled the degree of photocrosslinking and the corresponding mechanical properties of DLP-printed constructs.[58] The mechanical properties of the bioprinted tissue-mimics were varied from 6 to 8 kPa (liver) to 0.3–0.4 MPa (skin). Recently, we proposed a molecular cleavage approach, where hyaluronic acid methacrylate (HAMA) was mixed with GelMA to facilitate high-performance DLP bioprinting, followed by selectively enzymatic digestion of HAMA to achieve tissue-matching mechanical properties.[59] The stiffnesses were precisely tuned by adjusting the enzymatic digestion. We bioprinted multiple tissues from the muscles (42.9 kPa) to the brain (1.3 kPa), the softest organ of the human body, which displayed tissue-mimic architectures and tissue-matched stiffnesses with specific cell functions. It is important to be able to achieve a wide range of mechanical properties of bioprinted constructs, replicating tissue-specific mechanical features, potentially paving the way for broad applications in tissue and tissue model engineering.

BIOINKS

The selection of bioinks applied toward SLA/DLP-based bioprinting depends on several factors. The biomaterials need to solidify quickly under the patterning light, and thus the bioinks are limited to the photocurable biomaterials that are functionalized with photocrosslinkable groups. In addition, as the light penetration affects bioprinting resolution, the opacity of the bioink requires to be considered. Moreover, more viscous bioinks usually result in longer fabrication times because they are slower to refill between the adjacent layers. Bioinks can be classified into two categories: natural bioinks and synthetic bioinks (Table 1). To build bioscaffolds for tissue regeneration and *in vitro* modeling applications, natural bioinks may have advantages because of their intrinsic properties recapitulating the native ECM.[60] However, natural bioinks possess unpredictable variations among batches and are often too soft in mechanical properties to be bioprinted into 3D structures when used alone.[60]

Table 1. Typical bioinks used in SLA/DLP-based bioprinting

Biomaterials	Key advantages	Key disadvantages
Natural bioinks		
GelMA	Intrinsic RGD motifs	Thermogelling property Oxygen-inhibition Heterogeneous polymer networks Fast degradation
GelAGE	Fast reaction speed No oxygen-inhibition	Disulfide bond formation
HAMA	A component of ECM	Oxygen-inhibition Heterogeneous polymer networks
dECM	Tissue-specification	Weak mechanical properties
Sil-MA	Amino acids	Poor mechanical properties
Synthetic bioinks		
PEGDA	Proper mechanical properties	Limited cell-binding sites
PVA-MA	Low toxicity Hydrophilic property	Lack of cell-binding ligands
PGSM	Inexpensiveness Elastomeric nature	Limited mechanical properties Rapid degradation

Natural bioinks

GelMA

GelMA is one of the most widely used biomaterial ink derived from the natural source, which is synthesized by conjugating methacryloyl groups to gelatin, the hydrolysis product from collagen.[61] The synthesis process of GelMA includes the direct reaction of gelatin with methacrylic anhydride to substitute amine and hydroxyl groups with methacryloyl groups.[61]GelMA exhibits advantages in bioactivity and cell adhesion owing to the presence of intrinsic RGD motifs. The mechanical properties of GelMA can be adjusted by varying irradiation dose and its concentration during light-based crosslinking.[62] Taking advantage of the tunable mechanical properties, GelMA enables the fabrication of scaffolds with a wide range of stiffness values, mimicking a variety of tissues from the brain to liver and cartilage, and provides biomechanical guidance for cell migration and cell fate.[63] In DLP-based 3D bioprinting, to mimic the native stiffness of liver tissue, Ma et al. built the constructs with 5 w/v% GelMA encapsulating human induced pluripotent stem cell (hiPSC)-derived hepatic cells, where the matrix stiffness strongly influenced the hepatocytes functions.[64] In addition, applying GelMA in visible light-based DLP bioprinting with eosin Y as the photoinitiator, Wang et al. demonstrated that increasing GelMA concentration or Eosin Y concentration enhanced the mechanical properties of the fabricated NIH/3T3 hydrogel (Figure 3A), as well as improved cell attachment, but resulted in lower cell viability.[65] Therefore, the proper adjustments of construct stiffnesses are crucial to maintaining cell adhesions and viabilities of bioprinted cells and promoting stem cell differentiations.

GelMA also endows the thermogelling property, which benefits extrusion bioprinting due to the increased viscosity at low temperatures, allowing thermal crosslinking of the liquid bioink for keeping the 3D structural fidelity during extrusion.[70] However, the SLA/DLP method relies on the photopolymerization of liquid bioink within the vat in a layer-by-layer manner. It therefore requires that the bioink remains in the liquid state during the entire bioprinting process; this period varies from minutes to hours in SLA/DLP-based 3D bioprinting. Providing a thermostatic environment via a thermo-controlling system or reducing the GelMA concentration is possible to offset the thermogelling problem. Besides, fish-derived GelMA could be a promising material considering its lower gelling temperature and comparable physical properties with pork GelMA.[71–73] The high-resolution DLP printing of fish-derived GelMA (low-temperature-soluble GelMA) has been extensively illustrated in our study without temperature controls, allowing one to fabricate 3D structures embedded with complex channels and replicating anatomical 3D branches.[73]

However, as a protein from the natural source, uncertainty remains as to the features of GelMA including generally insufficient stiffness and fast degradation limit its use in SLA/DLP-based bioprinting. Therefore,

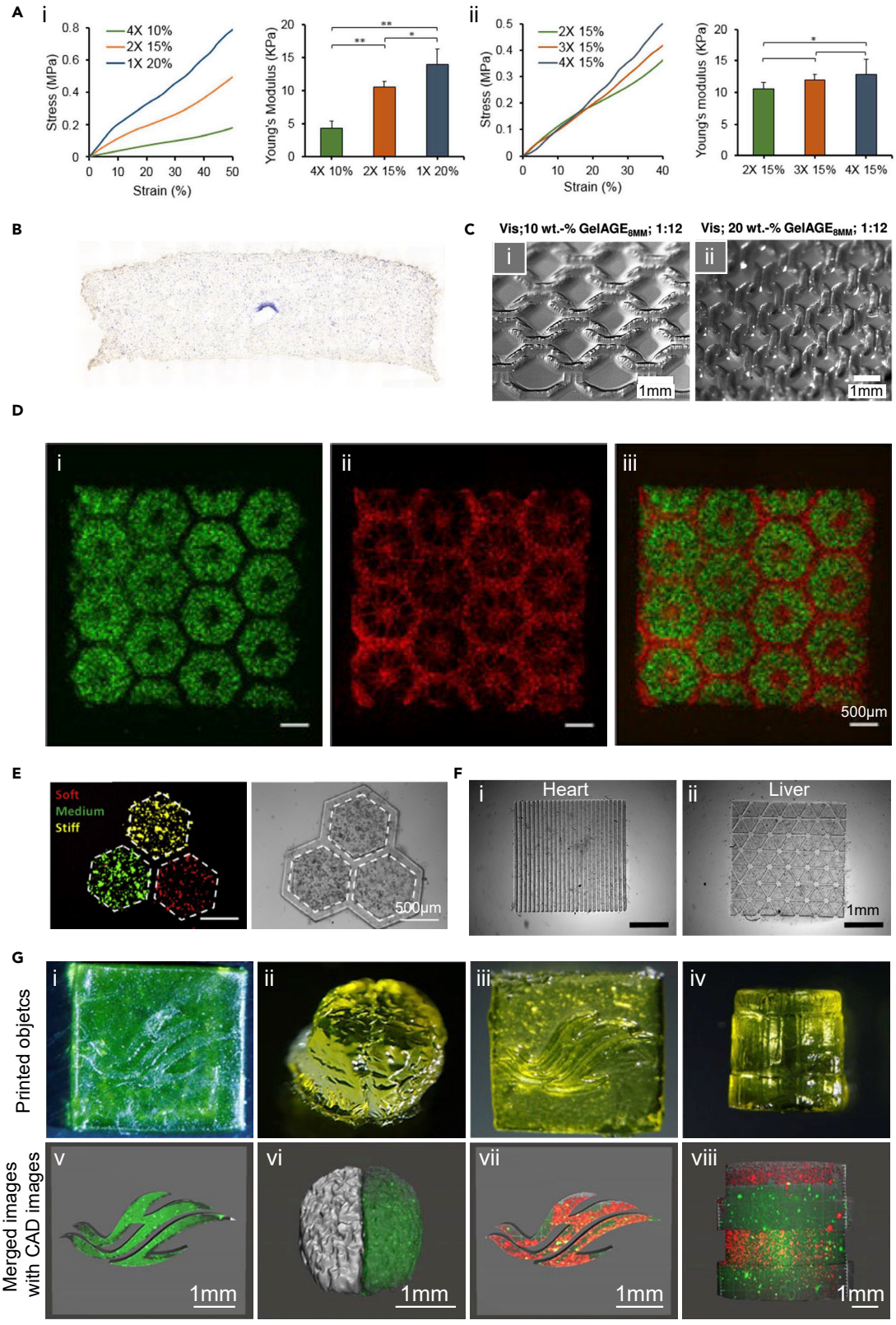
A
i
4X 10%
2X 15%
1X 20%
Stress (MPa)
Strain (%)
Young's Modulus (KPa)
4X 10%
2X 15%
1X 20%
ii
2X 15%
3X 15%
4X 15%
Stress (MPa)
Strain (%)
Young's modulus (KPa)
2X 15%
3X 15%
4X 15%
B
C
Vis;10 wt.-% GelAGE8MM; 1:12
Vis; 20 wt.-% GelAGE8MM; 1:12
1mm
1mm
D
500µm
E
Soft
Medium
Stiff
500µm
F
Heart
Liver
1mm
G
Printed objetcs
Merged images with CAD images
1mm
1mm
1mm
1mm

Figure 3. Natural bioinks employed in SLA/DLP-based bioprinting

(A) Strain-stress curves and Young's moduli of bioprinted GelMA constructs with varied (1) GelMA concentrations or (2) Eosin Y amounts (2). Reproduced with permission from.[65]

(B) Alkaline phosphatase (ALP) staining of MSCs in 3D GelMA/PEGDA hydrogel with a single channel cultured in osteogenic medium for 14 days. Reproduced with permission from.[42]

(C) Constructs fabricated by (1) 10 w/v% GelAGE and (2) 20 w/v% GelAGE using the visible light-initiated DLP platform. Reproduced with permission from.[66]

(D) Bioprinted hepatic structure of hiPSC-HPCs (green, i and iii) in 5 w/v% GelMA and HUVECs and adipose-derived stem cells (red, ii and iii) in 2.5 w/v% GelMA with 1 w/v% HAMA. Reproduced with permission from.[64]

(E) dECM-based bioprinting of liver model with varied mechanical properties. Fluorescence and bright-field images showing the distribution of HepG2/C3A cells assigned to hexagonal regions. Red indicates soft, green indicates medium, and yellow indicates stiff condition. Reproduced with permission from.[67]

(F) Bioprinting of 5 wt % dECM/GelMA (5/5 w/v%) constructs with heart and liver patterns. Reproduced with permission from.[68]

(G) 3D-bioprinted objects with Sil-MA (i-iv) and cell distributions in each object (v-viii). Reproduced with permission from.[69]

other components are combined with GelMA bioinks to increase the mechanics, which facilitates printability and pattern fidelity. For instance, PEGDA, as one of the most popular synthetic non-degradable materials used in tissue engineering, has been used in combination with GelMA to enhance the stiffness and structural integrity of bioprinted constructs. The hybrid bioink of GelMA/PEGDA (8/12 w/v%) successfully enabled DLP bioprinting of an MSC-laden hydrogel containing a single channel in the middle (Figure 3B).[42] The other photocrosslinkable and non-biodegradable materials, including alginate-methacrylate and carboxymethyl cellulose-methacrylate, which have been employed in the composites with GelMA for skeletal muscle engineering, could also be candidates in DLP 3D bioprinting with increased stiffness values and slower degradation profiles compared to pure GelMA.[74]

GelAGE

GelAGE is another gelatin-derived material with multifunctional thiol crosslinkers via the thiol-ene click reaction. Thiol-ene-based click reaction starts with the dimerization of thiols and carbon-carbon double bonds, followed by the step-growth manner with a high yield of functional groups, which enables low-initiator-concentration demands and fast reaction speeds.[75] Meanwhile, compared with the free-radical chain-growth photo-polymerization involved in methacrylate-functionalized biomaterials, the thiol-ene-based click reaction of GelAGE could overcome the obstacles in oxygen-inhibition and the formation of heterogeneous polymer networks.[75] However, the free thiol groups could undergo disulfide bond formation, which may compete with the thiol-ene click reactions in photopolymerization.[76] Bertlein et al. synthesized GelAGE through reacting gelatin with allyl glycidyl ether (AGE) by investigating different alkaline conditions, AGE concentrations, and reaction times.[66] The mechanical properties of the GelAGE hydrogel were changed significantly with varying synthesis conditions or adjusting the ratio of allyl and thiol from dithiothreitol (DTT). Furthermore, the DLP bioprinting system was utilized to fabricate 3D constructs with GelAGE via two different photoinitiators, Irgacure 2959 initiated by UV wavelength and Ru/SPS sensitive to the visible light. 10 and 20 w/v% GelAGE, synthesized with a medium concentration of NaOH (2.0 mmol) and medium concentration of AGE (12 mmol) in 8 h, printed porous constructs with 250-μm strands (Figure 3C). It is worthwhile mentioning that the lack of thermogelling feature of 10–20 w/v% GelAGE8MM at room temperature is important for SLA/DLP-based 3D bioprinting, which enables the bioink to maintain the liquid state. In addition, 20 w/v% GelAGE1MM displayed its biocompatible ability in bioprinting of human articular chondrocytes. Compared to the damage from UV irradiation during the crosslinking process, the cell viability was significantly increased with the visible light-based method.[66]

Methacrylated hyaluronic acid (HAMA)

Hyaluronic acid (HA) is a non-sulfated glycosaminoglycan, which is the component of ECM widely existing in epithelial, connective, and neuronal tissues.[77] HA can also be modified by conjugating methacrylate groups to form HAMA, which can be used for creating photocrosslinkable bioink formulations.[78] In combination with different materials, either natural or synthetic polymers, HAMA has been extensively used to enhance their printability and biological properties.[79] Using an SLA bioprinting system, HAMA was used as the bioink to encapsulate chondrocytes, where the cells remained viable and were able to differentiate into cartilage-mimicking tissues after 14 days.[80] A recent study conducted by Ma et al. with DLP bioprinting, showed that a mixture of HAMA (1 w/v%) and GelMA (2.5 w/v%) served as the bioink encapsulating endothelial cells and mesenchymal cells in a liver model because HAMA was capable of promoting the proliferation of endothelial cells and vascularization (Figure 3D).[64]

dECM

ECM is the 3D extracellular network in the body and is mainly composed of collagen, glycoproteins, and enzymes to support cellular functions in both structural and biochemical manners.[81] As the ECM is specific for the different tissue types, the dECM obtained from tissue digestion is an ideal material to recapitulate the complex microenvironment of the target tissue.[82,83] To harvest tissue-specific dECM, the desired tissue needs to be processed by physical breakdown, enzymatic digestion, and chemical wash to collect the ECM without cells.[84] Various studies verified that the bioengineered dECM was able to fabricate scaffolds with enhanced biological performances. For example, Ma et al. bioprinted the dECM constructs with varied stiffness through modulating the different exposure times (Figure 3E).[67] This bioprinted *in vitro* model was applied to mimicking liver cancer under the fibrotic environment and to investigate cell invasion and growth. Further study was conducted by Yu et al. using the heart or liver dECM loaded with hiPSC-derived cardiomyocytes or hepatocytes to fabricate the corresponding tissues.[68] However, none of these studies can solve the weak mechanical issue of dECM, resulting in poor bioprinting fidelity and limiting its application on SLA/DLP bioprinting. To overcome this problem, Yu et al. prepared the modified bioink by adding 5 w/v% GelMA into 5 w/v% dECM to produce tissue scaffolds using the DLP system. They successfully bioprinted constructs encapsulated with hiPSC-derived cardiomyocytes or hepatocytes with tunable mechanical properties by modulating the crosslinking time (Figure 3F).[68]

Methacryloyl-modified silk (Sil-MA)

Silk fibroin, derived by silkworm *Bombyx mori*, is a natural fibrous protein and contains a repeating pattern of amino acids. It has been used in biomedicine as the material for wound dressing, implants, and vascular prostheses, among others.[85] Most of the silk-derived materials have displayed poor mechanical properties compared to native silk fibers owing to the degumming and dissolution processes. Through covalent conjugation of methacryloyl groups to amines of silk fibroin, Sil-MA could be photocrosslinked and showed enhanced mechanically after photopolymerization.[69,86] Kim et al. utilized Sil-MA as the bioink to fabricate porous constructs via the DLP bioprinting method (Figure 3G).[69] Rapid fabrication times guaranteed the cells to remain undamaged and well-distributed with further proliferation. Moreover, mechanical properties of Sil-MA hydrogels could be tuned by changing the methacrylation degrees and the macromer concentrations.

Other potential photocurable bioinks

Collagen is the ECM protein abundantly distributed in tissues and is beneficial for cell proliferation, differentiation, and adhesion in tissue engineering.[87] Drzewiecki et al. proposed collagen methacryloyl (ColMA) by reacting with methacrylic acid and collagen using *N*-hydroxysuccinimide (NHS) and 1-ethyl-3-[3-(dimethylamino)propyl] carbodiimide (EDC). ColMA has been proven to be photocrosslinked when exposed to the 365-nm UV light and could maintain its thermogelling property.[88] In addition, alginate is obtained from the alginate salt collected from brown algae.[89] To achieve the light-based printability, methacrylated alginate is prepared by the reaction with 2-aminoethyl methacrylate. Methacrylated alginate was photocured by UV irradiation and showed biocompatibility with chondrocytes.[90] Its mechanical properties and degradation rates varied with different methacrylation degrees. Furthermore, chitosan, derived from chitin, is a natural polysaccharide distributed widely in the exoskeleton of crustaceans and insects.[91] With the introduction of the allyl group, the modified chitosan was crosslinked under the UV light in less than a minute.[92] These photocurable materials demonstrated the potential capability of applications on SLA/DLP-based 3D bioprinting, enabling them to fabricate complex constructs with higher resolution effectively.

Synthetic bioinks

PEGDA

Poly(ethylene glycol) (PEG), as a hydrophilic, biocompatible, and water-soluble polymer, has been investigated in numerous biomedical and clinical applications.[93]PEGDA-based biomaterial bioink is the most commonly used system to fabricate high-resolution constructs with SLA/DLP because of its ability to undergo rapid light-induced photopolymerization and assume proper mechanical properties.[51] However, the limited protein binding sites on PEGDA leads to poor cell attachment on the printed PEGDA scaffolds, hindering its application in biomedicine. To overcome this obstacle, strategies of modifying PEGDA with cell-adhesive components are proposed, for example, with hexapeptide and RGD peptides, which have been shown to enhance cell survival, attachment, and spreading on the printed PGEDA scaffolds.[94]

The other biomaterials possessing cell-adhesive properties, such GelMA, are also utilized to incorporate with PEGDA for DLP-based bioprinting.[95] Koffler et al. bioprinted the 3D spinal cord using the DMD-based microscale continuous projection (μCPP) platform.[96] The bioprinted construct containing channels with 200-μm-diameter provided biological guidance for the axon growth. The scaffold fabricated by the GelMA/PEGDA (7.5 w/v%/25 v/v%) bioink encapsulating neural progenitor cells (NPCs) was proven to well-integrate into the injury site. In this study, it was also claimed that the GelMA/PEGDA-bioprinted construct exhibited the slower degradation *in vivo*, compared with the HA-based scaffold, which was necessary for axon regeneration and could provide long-term physical support *in vivo*. In addition, Miller and co-workers used PEGDA to build sophisticated 3D constructs with the DLP approach.[42] They successfully printed an acellular vascularized alveolar unit that enabled mimicking the breath function (Figure 4A). By mixing GelMA (7.5 w/v%) with PEGDA (7.5 w/v%), they also bioprinted the functional hepatic tissue-mimic containing hepatocyte aggregates and endothelial cells for *in vivo* implantation and regeneration.

Poly(vinyl alcohol) methacrylate (PVA-MA)

Poly(vinyl alcohol) (PVA) is advantageous in terms of low toxicity and the hydrophilic nature, which is also easily modified with various functional groups because of the abundant hydroxyl groups on PVA.[99] Lim et al. utilized the photocurable PVA-MA to bioprint 3D constructs with the high resolution of 25–50 μm via the visible light-based DLP approach (Figure 4B).[97] In this study, GelMA was integrated into the PVA-MA bioink for the purpose of enhancing the biocompatibility and cell-attachment of PVA. The results confirmed that bioprinted scaffolds with GelMA/PVA-MA (1/10 w/v%) supported the encapsulated endothelial cell spreading and promoted osteogenic and chondrogenic differentiations of MSCs.

Poly(glycerol-co-sebacate) (PGS)-methacrylate (PGSM)

PGS is the copolymer of sebacic acid and glycerol, which is broadly applied for use in numerous US Food and Drug Administration (FDA)-approved medical devices.[100] PGS displays good biocompatibility and rapid degradation under physiological conditions.[101] It has been demonstrated by many studies that PGS is a promising material in biomedical applications, including cardiac tissue engineering, fabrication of vascular conduits and retinal implants, as well as skin, cartilage, and neural regeneration.[101,102] PGSM is a PGS-derivative and photocrosslinkable with light-based printing systems.[98] Singh et al. utilized PGSM synthesized by reacting with methacrylic anhydride, to fabricate the 3D nerve guidance conduits through the DLP method.[98] The mechanical properties and degradation rates of the printed PGSM could be adjusted by varying concentrations of methacrylic anhydride during PGSM synthesis. To achieve the tissue-matching mechanical property with natural nerve and obtain a slow degradation, the formulation of 75% as a degree of methacrylation was selected to print conduits with stiffness of approximately 3 MPa. The following *in vivo* implantation studies revealed that the printed conduits promoted axon regeneration in the mouse fibular nerve injury model (Figure 4C).

APPLICATIONS OF SLA/DLP-BASED BIOPRINTING

The combinations of viable cells and proper biomaterials have been used as the bioinks in 3D bioprinting because the distribution of cells can be precisely controlled to gather complex and heterogeneous structures with cell-cell and cell-matrix interactions.[2] It allows us to replicate biological tissues and mimicking specific functions for diverse biomedical purposes. Given the favorable properties of bioprinting solution and capacities of fabricating highly complex constructs, SLA/DLP-based 3D bioprinting holds great value in tissue modeling and regenerative medicine aspects.[103]

Tissue modeling

3D *in vitro* models have been extensively investigated in the biomedical field due to their potentials in the studies of cell interactions, understanding of pathogenesis, as well as utilities in drug screening.[104] They have been extensively developed over the past decade attributed to improvement in bioprinting techniques, as a means for supplementing or replacing animal models in the preclinical drug-development phases, the latter of which oftentimes feature high costs and uncertainties in bridging with the human physiology.[105] It is noteworthy to mention that the SLA/DLP-based bioprinting methods have increasingly contributed to fabricating a range of biomimetic human tissue models (Table 2), replicating the delicate architectures, complex compositions, and functions of the relevant *in vivo* counterparts.

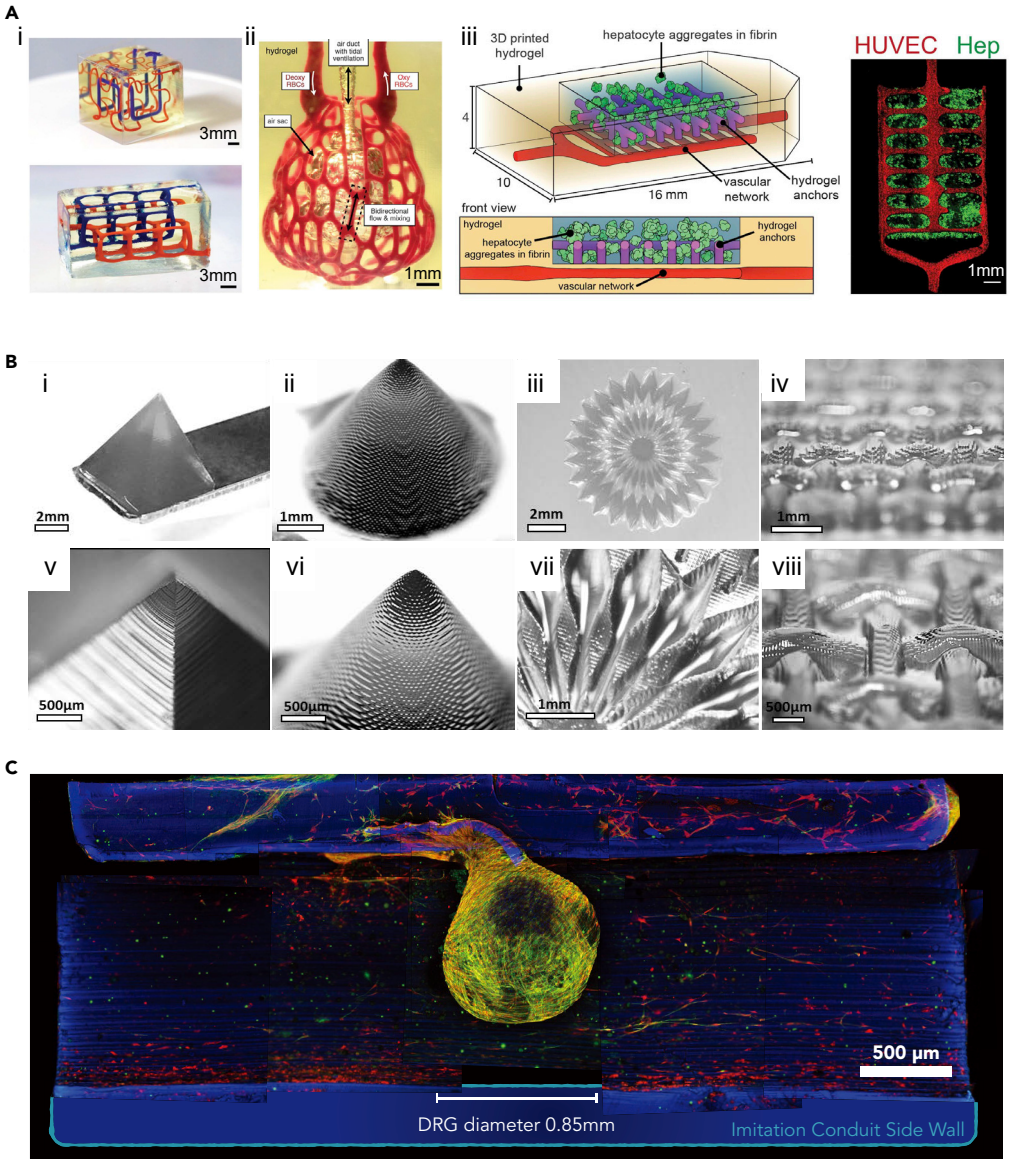

Figure 4. Synthetic bioinks applied in SLA/DLP-based bioprinting

(A) i-ii, non-cellular 3D constructs printed with PEDGA, including (i) entangled vascular networks and (ii) vascularized alveolar unit. (iii) Prevascularized hepatic hydrogel bioprinted using GelMA/PEGDA presenting HUVECs (red) in the vascular network and hepatocyte aggregates (Hep, green). Reproduced with permission from.[42]

(B) Fabrications of PVA-MA constructs with a high resolution. The 50-μm voxel step size showing in enlarged images. Reproduced with permission from.[97]

(C) PGSM-printed nerve guidance conduit (NGC) in blue, and the dorsal root ganglion (DRG) seeded on the NGC, where Schwann cells labeled with anti S100B in red, neurites with anti β-III-tubulin in green. Reproduced with permission from.[98]

The co-culture systems within 3D-bioprinted structures encapsulating different cell types have been widely established using the SLA/DLP approaches, aiming to reveal cellular interactions. Zorlutuna et al. developed oxidized methacrylated alginate hydrogel combined with PEG-methacrylate (OMA-PEGDA) to examine the interactions between primary hippocampus neurons and skeletal muscle myoblasts (Figure 5A).[106] Bioink containing skeletal muscle myoblasts was bioprinted under UV light using the SLA method in a torus form, and the hippocampus neuron-encapsulating bioink was subsequently fabricated inside the hydrogel of skeletal muscle myoblast torus. The functionality of neurons within the hydrogel was verified through their choline acetyltransferase (ChAT) activities over 10 days of culture,

Table 2. Selected applications of SLA/DLP-based bioprinting in tissue modeling

Modeltype	Printing system	Biomaterials	Cells	Advantages	Reference
Co-culture of neurons and muscle myoblasts	UV-enabled SLA	Oxidized methacrylic alginate (OMA)-PEGDA	Primary hippocampus neurons and skeletal muscle myoblasts	Functionality of neurons was promoted in 3D when co-cultured with skeletal muscle myoblasts	Zorlutuna et al.[106]
Breast cancer model	UV-enabled SLA	GelMA and nHA	MSCs or human osteoblasts, and BrCa cells	Post-metastatic breast cancer progression in the bone microenvironment	Zhou et al.[107]
GBM environment model	Multi-material UV-enabled DLP	GelMA and HAMA	GSCs, macrophages, NPCs, and astrocytes	Interactions between tumor and immune cells	Tang et al.[108]
Tri-regional GBM model	Multi-material UV-enabled DLP	GelMA and HAMA	GBM cells and HUVECs	Tri-regions of GBM, brain parenchyma, and surrounding capillaries with regional stiffnesses	Tang et al.[109]
3D triculture liver model	UV-enabled DLP	GelMA; GelMA and HAMA	hiPSC-HPCs; adipose-derived stem cells and HUVECs	Liver model with hepatic lobule structure presented hepatic functions	Ma et al.[64]
Liver model of HCC	UV-enabled DLP	dECM	HepG2/C3A cells	HCC model with tailorable mechanical properties	Ma et al.[67]
Cardiac model	UV-enabled DLP	GelMA	NMVCMs	NMVCMs bioprinted in linear patterns aligned as myofibril	Liu et al.[110]

where the highest expression was detected in the scaffold of 3D co-cultured with skeletal muscle myoblasts.

In the tumor microenvironment, cancer progression and metastasis involve complex interactions between tumor cells and the surrounding stromal compartment. The SLA/DLP bioprinting procedures have been employed to study the crosstalk among stromal cells, tumor cells, and/or immune cells, understanding stromal-tumor signaling in tumor cell behaviors and metastasis. For example, the bone matrices composed of MSCs or human osteoblasts in GelMA mixed with nanocrystalline hydroxyapatite (nHA) were bioprinted using UV light-based SLA method (Figure 5B).[107] The breast cancer (BrCa) cells seeded onto these bioprinted GelMA scaffolds implied the enhanced cell metabolic activities and the increased secretion of vascular endothelial growth factor (VEGF). Meanwhile, the cell proliferation and alkaline phosphatase activities of osteoblasts/MSCs were inhibited by the BrCa cells. Thus, it was concluded that the 3D-bioprinted scaffolds containing BrCa cells and bone stromal cells provided an *in vitro* model for studying post-metastatic breast cancer progression in the bone microenvironment. Additionally, a 3D glioblastoma (GBM) microenvironment model was created using the two-step multi-material DLP-based bioprinting (Figure 5C).[108] The GelMA/HAMA (4/0.25 w/v%) bioink encapsulating GBM stem cells (GSCs) and macrophages were bioprinted as the tumor core, whereas the bioink containing NPCs and astrocytes was applied to construct the peripheral region. The HA-based bioink supplied microenvironmental cues, together with multiple cell components, which allowed one to render a highly reproducible model for GBM biology. More importantly, applying this rapid DLP bioprinting platform, the functions of macrophages in GBM, as well as the cell interactions between tumor and immune cells, were convenient to be investigated through adding or removing macrophages from the bioink, which could not be easily achieved in conventional xenograft or genetically modified mouse models. The results demonstrated from this *in vitro* model where the addition of macrophages activated the invasive behaviors of GBM served as a more practical platform for drug testing. Meanwhile, the polarization of macrophages to the protumoral M2 macrophage phenotype was enhanced, suggesting the bidirectional crosstalk within the 3D GBM microenvironment model. Furthermore, the same group used the similar DLP technology by sequentially adding multiple bioinks. A biomimetic tri-regional GBM model consisted of tumor region, acellular ECM region, and endothelial region with regional stiffnesses patterned regarding GBM, brain parenchyma, and surrounding capillaries was fabricated (Figure 5D).[109] To obtain the regionally varied biophysical properties, the tumor region of GBM cells was bioprinted with 5 w/v% GelMA and 1 w/v% HAMA, the endothelial part was fabricated using 2.5 w/v% GelMA and 0.5 w/v% HAMA, and the ECM was patterned by 5 w/v% GelMA

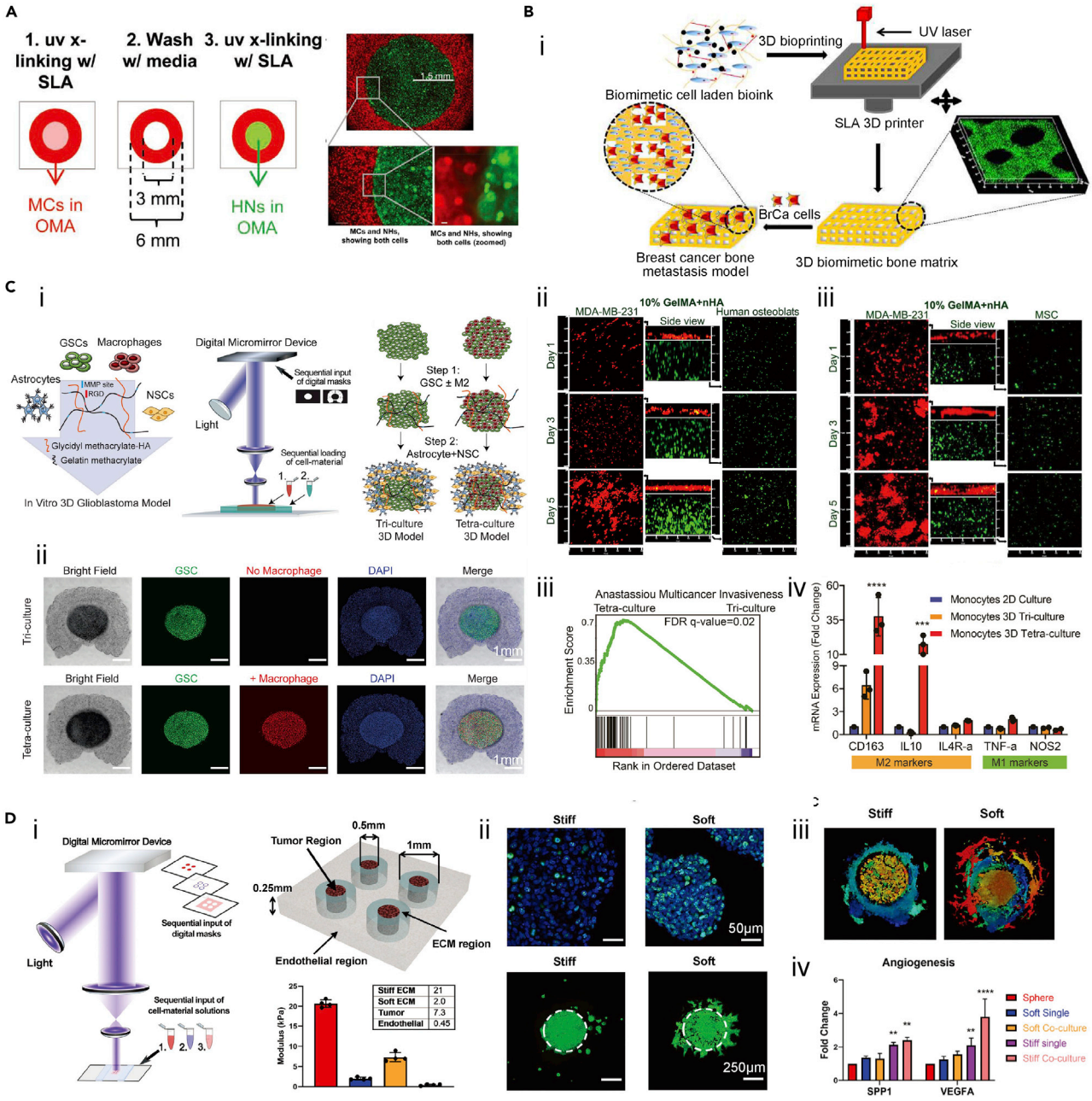

Figure 5. Applications of SLA/DLP-based bioprinting for cell-interaction studies

(A) 3D-bioprinted construct to mimic the interactions between primary hippocampus neurons and skeletal muscle myoblasts. Reproduced with permission from.[106]

(B) A 3D-bioprinted bone matrix as a biomimetic model. (i) Schematic showing 3D-bioprinted bone construct for breast cancer metastasis study. (ii) Confocal images showing osteoblasts and BrCa co-cultured in the bioprinted scaffold after 1, 3, and 5 days. (iii) Confocal images showing MSCs and BrCa cells co-cultured in the bioprinted scaffold after 1, 3, and 5 days. Reproduced with permission from.[107]

(C) 3D-bioprinted GBM model through DLP method. (i) Schematic showing the *in vitro* 3D-bioprinted GBM model containing macrophages, GSCs, astrocytes, and NSCs. (ii) Brightfield and immunostaining result of the tri-culture and tetra-culture 3D GBM models. (iii) Gene set enrichment analysis (GSEA) of multicancer invasiveness pathway in the GBM model with tetra-culture and tri-culture conditions. (iv) The mRNA expressions of M1 and M2 macrophage phenotype markers in different culture conditions. Reproduced with permission from.[108]

(D) 3D bioprinting of GBM *in vitro* model. (i) Bioprinter schematic and design of 3D-bioprinted GBM model with regionally varied biophysical properties. (ii) ki67 immunostaining (up) and invasion patterns (down) of TS576 cells in different stiffness of bioprinted constructs. (iii) Invasion patterns of TS576 cells in 3D co-culture models. (iv) mRNA expressions of angiogenesis markers of TS576 cells in different culture conditions. Reproduced with permission from.[109]

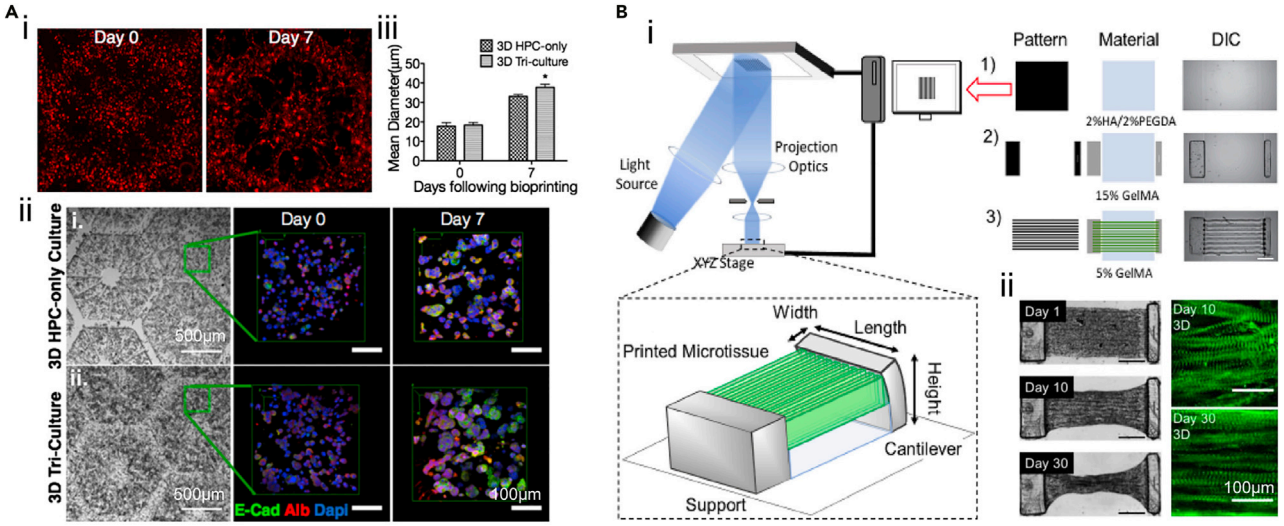

Figure 6. Applying SLA/DLP-based bioprinting for liver and cardiac microtissues modeling

(A) Characterizations of 3D-bioprinted *in vitro* hepatic model. (i) Fluorescence images showing cell distributions at day 0 and day 7. (ii) Brightfield and confocal images revealing albumin and E-cadherin, and nucleus staining of hiPSC-HPCs cultured in HPC-only scaffolds and 3D triculture samples. (iii) Mean diameters of hiPSC-HPCs spheroids cultured in HPC-only and 3D triculture constructs at day 0 and day 7. Reproduced with permission from.[64]

(B) DLP-based bioprinting of 3D cardiac tissue. (i) Design of 3-layered bioprinted scaffold for cardiac tissue supporting. (ii) Compaction and α-actinin staining of bioprinted cardiac tissues. Reproduced with permission from.[110]

and 0.5 w/v% HAMA (stiff) or 2.5 w/v% GelMA and 0.5 w/v% HAMA (soft). The two ECM formulations with different stiffness (stiff and soft) were designed for replicating the conditions of healthy brain parenchyma or GBM-remodeled stroma. They demonstrated increased cell proliferation and expansion in the soft ECM, but the stiff model promoted the malignant phenotypes, such as hypoxia, stemness, and angiogenic potentials. Integration of vascular component enabled them to observe the sprouting and proliferation of endothelial cells in the GBM model, where the human umbilical vein endothelial cells (HUVECs) proliferation was apparent on the soft substitute, and both sprouting and proliferation were presented in the stiff scaffold. In this study, the DLP-based bioprinting platform allowed to fabricate of GBM models with biophysical heterogeneity in a rapid, flexible, and reproducible manner, which could be employed as a potential system for the patient-specific GBM modeling and drug screening.

DLP-based bioprinting has also been applied toward creating tissue mimics possessing organ-specific geometries, such as liver and cardiac tissues,[111,112] attributing to the reproduction of sophisticated architectures. Ma et al. utilized hiPSC-derived hepatic progenitor cells (hiPSC-HPCs) and bioprinted the liver model with a UV-enabled DLP bioprinting system (Figure 6A).[64] They bioprinted hiPSC-HPCs with 5 w/v% GelMA as the liver lobule structure and adipose-derived stem cells and HUVECs embedding in 2.5 w/v% GelMA and 1 w/v% HAMA to be the vascular pattern. The hepatic functions were further evidenced by liver-specific gene expressions, hepatic functional indicators, including albumin and urea secretions, and the cytochrome P450 induction. Compared to the 2D-cultured hiPSC-HPCs and the 3D-bioprinted liver model without vascular components, the developed 3D triculture liver model presented the promoted phenotypic and functional behaviors, suggesting that the 3D biomimetic liver model could be potentially applied for disease modeling and drug screening studies. The same team also built a liver model using the dECM with DLP approach, which featured tailorable mechanical properties for the model of hepatocellular carcinoma (HCC).[67] HepG2/C3A cells encapsulated in bioprinted dECM-scaffolds possessing a cirrhotic range of stiffness exhibited reduced cell growth as well as increased invasion markers compared to healthy controls. Besides the geometric replication, the cirrhosis-relevant stiffness could be obtained by adjusting the exposure time of bioprinting, further promoting the cell behaviors of disease conditions.

In another example, Liu et al. bioprinted the *in vitro* cardiac model by the three steps of the method (Figure 6B).[110] The base layer of this design was patterned with 2 w/v% HAMA and 2 v/v% PEGDA, followed by the bioprinting of pillar structure using 15 w/v% GelMA. Finally, the neonatal mouse ventricular cardiomyocytes (NMVCMs) were incorporated into 5 w/v% GelMA and bioprinted by the line pattern. The designed

Table 3. Selected applications of SLA/DLP-based bioprinting in regenerative medicine

Modeltype	Printing system	Biomaterials	Cells	Advantages	Reference
Cartilage tissue	DLP with blue light	GelMA or HAMA	Chondrocytes	GelMA scaffold facilitated chondrocyte phenotype	Lam et al.[80]
Cartilage tissue	UV-enabled DLP	Silk-GMA	Chondrocytes	Cartilage tissue repair of partially defected trachea rabbit model	Hong et al.[113]
Vascularized liver tissue	UV-enabled DLP	GelMA and HAMA; GelMA	HUVECs; hiPSC-HPCs	Anastomosis between host circulation and bioprinted scaffold	Zhu et al.[114]
Spinal cord	UV-enabled DLP	GelMA/PEGDA	Seeding NPCs	Spinal cord with patient-specific shape presented *in vivo* integration	Koffler et al.[96]

model enabled to achieve an asymmetric, multi-material, cantilever-based construct, allowing one to produce and transmit force onto a single deformable pillar. Therefore, the encapsulated NMVCMs in linear patterns with geometric cues formed rod-shaped morphology and aligned as myofibril phenotypic of the myocardium. In comparison to the 2D-cultured cells, the aligned NMVCMs bioprinted within 3D hydrogel displayed nearly 2 times of forces in mechanical evaluations, as well as increased characteristic calcium transient waveforms. This study generated the myofibril alignment phenotype by tuning the scaffold microarchitectures, providing physiologically relevant models for cardiac disease modeling and drug development.

Regenerative medicine

The SLA/DLP-based bioprinting methods enable the construction of complex geometries with high resolutions for producing implantable scaffolds and advanced tissue replacements ranging from the vasculature to the neural networks (Table 3), with tunable physicochemical properties that are highly applicable for clinical applications. The 3D-bioprinted constructs serve as biomimetic scaffolds with the desired physicochemical features and cellular components to support functionality reconstructions.

To create artificial cartilage *in vitro*, Lam et al. bioprinted the cartilage-mimic structures with GelMA or HAMA-based bioink by the DLP-based process.[80] Scaffolds made of GelMA or HAMA supported cartilage ECM formation and the viability of chondrocytes over 14 days of culture. GelMA-bioprinted samples exhibited a higher level of alpha-1 type I collagen (COL1A1) expression compared to HAMA-bioprinted scaffolds, suggesting the more premature chondrocyte phenotype facilitated by GelMA (Figure 7A). Moreover, silk fibroin functionalized with glycidyl methacrylate (silk-GMA) was also used to encapsulate chondrocytes and build cartilage tissue by Hong et al. using DLP-based bioprinting.[113] Cell-laden silk-GMA hydrogels displayed good cell viability, proliferation, and chondrogenic differentiation after 4 weeks of culture. Moreover, the bioprinted scaffolds were transplanted to the partially defected trachea rabbit model, which achieved excellent cartilage tissue formation over 6 weeks (Figure 7B). Therefore, the DLP technique could be applied to producing cartilage tissue substitutes to treat articular cartilage defects utilizing selected bioinks and patient-specific shapes.

Given the observed successful reconstruction of solid tissues with DLP bioprinting, the extension of its application for constructing vascularized tissues should also be taken into account. Vascular networks play a pivotal role in tissue engineering due to their capacities to transport nutrients and oxygen, as well as in eliminating metabolic wastes. To incorporate vasculature into tissue scaffolds, DLP-based bioprinting was applied to build a vascularized liver tissue, where a mixture of 2.5 w/v% GelMA and 1 w/v% HAMA was bioprinted into the vascular region containing HUVECs, and 5 w/v% GelMA with hiPSC-HPCs was utilized to construct the surrounding region.[114] These lumen-like structures formed in the vascular areas were verified both *in vitro* and *in vivo* (Figure 7C). Meanwhile, anastomosis between endothelial networks in the bioprinted scaffold and the host circulation was observed by perfusable blood vessels featuring red blood cells. The advanced approach of introducing vascular structures with faster bioprinting speed and complex geometries can be widely employed to fabricate diverse functional tissues.

As one of the most critical tissues, bioprinting studies related with the central nervous system (CNS) are limited because of the complexity of CNS architectures. Taking advantage of the high resolution of DLP-based 3D bioprinting, a spinal cord scaffold was fabricated and verified by implanting into rats with T3 complete the spinal cord transection.[96] Facilitated by the digital images obtained from processing

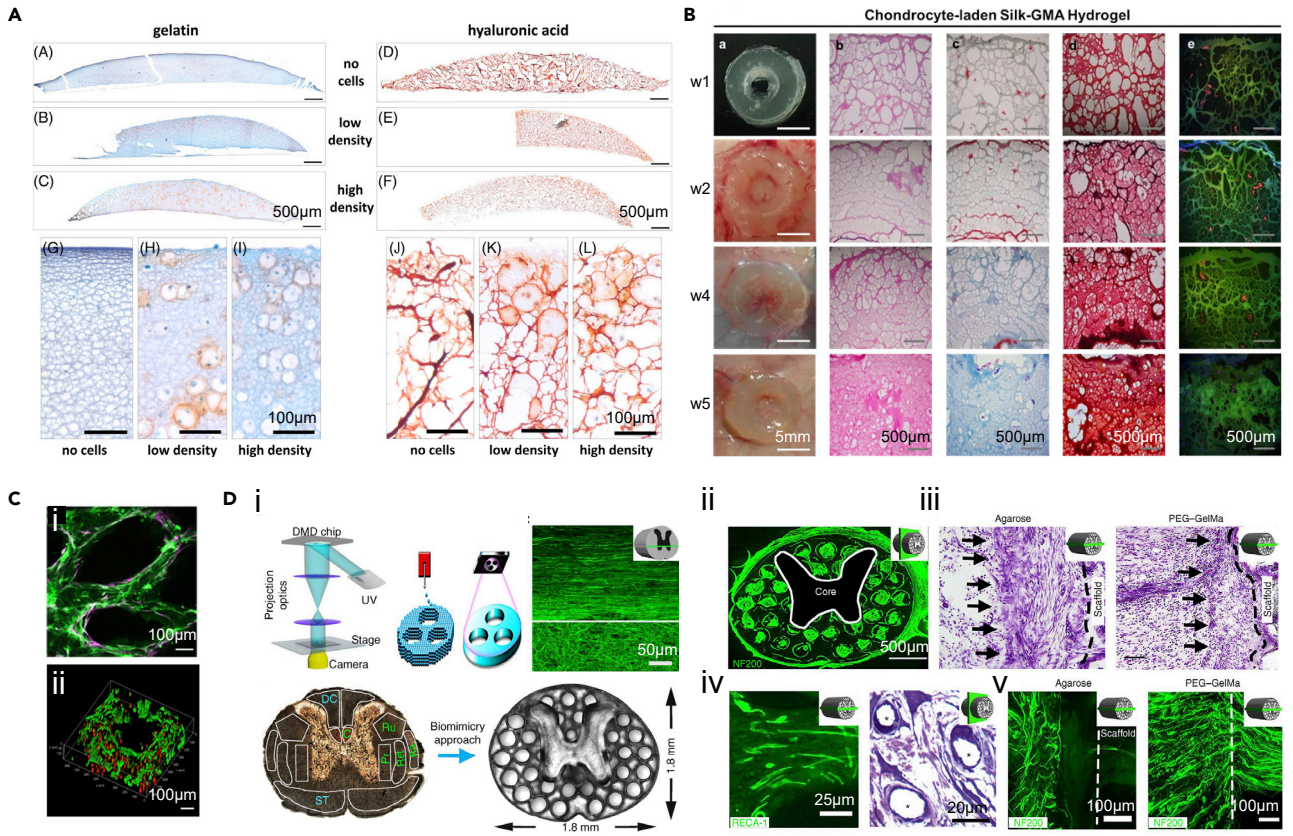

Figure 7. The SLA/DLP-based bioprinting facilities regenerative medicine

(A) Expressions of proteoglycans in bioprinted constructs with different chondrocyte densities after 14 days of culture. Reproduced with permission from.[80]

(B) *In vivo* histological assessments of chondrocyte-laden silk-GMA constructs for cartilage tissue regeneration after 1, 2, 4, and 5 weeks of implantation in dorsal subcutaneous part of mice. Reproduced with permission from.[113]

(C) Endothelial network formation of GelMA/HAMA constructs after 1-week culture *in vitro*. Reproduced with permission from.[114]

(D) The 3D-printed scaffold for spinal cord regeneration. (i) Schematic of DLP printing process and spinal cord scaffold design. (ii) Cross-section of the implanted scaffold labeled with axons (green). (iii) Nissl staining indicating the cell layer at the region of implantation. (iv) Toluidine blue stain (asterisks indicate vessels) (right) and RECA-1 immunolabeling (left) showing the vascularization of implanted scaffolds. (v) Host axons did not enter the agarose scaffold, whereas they could enter the 3D-printed GelMA/PEGDA scaffold. Reproduced with permission from.[96]

the cross-sectional images of the spinal cord, the gray matter was printed as solid with 7.5 w/v% GelMA and 25 w/v% PEGDA, and the channels of 200 μm in diameter were fused into the white matter to implement linear administration for the axonal reconstruction (Figure 7D). After 1 month of transplantation, NPCs loaded to the printed scaffolds directly after implantation could survive and completely fill the printed channels to support axon regeneration. Meanwhile, the host axons near the grafts regenerated into 3D-printed scaffolds and the implanted NPCs in turn extend axons out of the scaffold into the host spinal cord. These scaffolds can be scaled to any patient-specific lesion shape and length, providing great potential to repair and regenerate these injuries tailored to personalized patient requirements.

FUTURE PERSPECTIVES

In biomedicine, SLA/DLP bioprinting exhibits unique advantages such as the faster fabrication speeds, the accurate control over scaffold geometries, and preferrable resolutions. Utilizing the clinically relevant graphical information to create patient-specific anatomical, combined with the stem cell technology, advanced SLA/DLP bioprinting systems hold the potential of developing tissue replicates and disease models for the development of therapeutic approaches that are possibly personalizable.

Drug discovery is both capital- and time-intensive, yet the failure of therapeutic development involves the poor transition of *in vitro* screenings and preclinical animal models to human translations. 3D-bioprinted

engineered tissue constructs have gained increasing attention for *in vitro* modeling in recent years. SLA/DLP bioprinting offers the potential to approach the complexities of tissue architectures in an effective and repeatable manner. Besides the biomimetic macrostructures attainable from SLA/DLP bioprinting, challenges remain in simultaneously incorporating all physiologically relevant features, such as electrical conductivity. Qi and colleagues presented a hybrid multi-material 3D printing system by combining the DLP method and direct ink writing (DIW) printing.[115] The conductive inks were printed via DIW, whereas the acrylate-based materials were printed through DLP, which enabled fabricating of composite structures with conductivity. Future advancements in printing techniques and materials will expand the capacity of fabricating physiologically relevant physical, chemical and biological features.

Moreover, the potential high throughput is another promising advantage that DLP bioprinting can contribute to drug screening. Chen and colleagues extended the DMD-based DLP method to rapidly fabricating sophisticated 3D microtissues in the multi-well plate format, including those of hepatocellular carcinoma and human iPSC-derived cardiac microtissues, which is potentially beneficial in preclinical drug screening and disease modeling.[116,117] However, advancements in both *in vitro* maintenance and analysis systems will be needed to fully realize the potential of 3D bioprinting in developing *in vitro* disease models and precision medicine. Bioreactors and microfluidic devices provide possibilities for culturing bioprinted 3D microtissues, promoting nutrient supplement and functional maturation, especially for the volumetric tissues. In addition, based on the imaging and analyzing tools developed in the planar organ-on-chip systems, further advances of *in situ* assays of drug responses of organ-on-chips will facilitate to monitor of metabolism and many other key physiological parameters in real-time. The dynamic circulation technique will also be in high demand to connect multiple organ-mimics, eventually approaching the human-on-a-chip and serving as a class of new higher-throughput drug development platforms to study the interdependent effects of different organs.

Finally, surgical procedures usually result in several inherent drawbacks, such as extended hospitalization, anesthetic use, pain, swelling, and prolonged recovery. Therefore, developing minimally invasive or noninvasive approaches is a notable trend of clinical interventions. As the technology continues to develop, it can be predicted the minimally invasive 3D bioprinting can be achieved to directly pattern in living tissues. Recently, a digital near-infrared (NIR) photopolymerization system was developed to minimally invasively fabricate 3D constructs *in vivo* through DLP-based bioprinting.[118] Without needing open surgery-enabled implantation, the subcutaneously injected bioink could be noninvasively patterned layer-by-layer into personalizable structures *in vivo* for tissue repairing. *In vivo* bioprinting opens new avenues for the clinical translations of DLP bioprinting for producing patient-specific constructs and beyond.

ACKNOWLEDGMENTS

This work was supported by funding from the National Institutes of Health (R21EB025270, R21EB026175), the National Science Foundation (CBET-EBMS-1936105, CISE-IIS-2225698), and the Brigham Research Institute. A.O.L acknowledges the National Council for Scientific and Technological Development (CNPq, #310883/2020-2, #404683/2018-5) for financial support. We further thank Ami Lesha for proofreading the manuscript.

DECLARATION OF INTERESTS

Y.S.Z. consults for Allevi by 3D Systems, and sits on the scientific advisory board and holds options of Xellar, both of which however, did not participate in or bias the work. The other authors declare no competing interests.

REFERENCES

1. Murphy, S.V., and Atala, A. (2014). 3D bioprinting of tissues and organs. Nat. Biotechnol. *32*, 773–785. https://doi.org/10.1038/nbt.2958.

2. Gungor-Ozkerim, P.S., Inci, I., Zhang, Y.S., Khademhosseini, A., and Dokmeci, M.R. (2018). Bioinks for 3D bioprinting: an overview. Biomater. Sci. *6*, 915–946.

3. Landers, R., Hübner, U., Schmelzeisen, R., and Mülhaupt, R. (2002). Rapid prototyping of scaffolds derived from thermoreversible hydrogels and tailored for applications in tissue engineering. Biomaterials *23*, 4437–4447.

4. Wilson, W.C., and Boland, T. (2003). Cell and organ printing 1: protein and cell printers. Anat. Rec. A Discov. Mol. Cell. Evol. Biol. *272*, 491–496.

5. Boland, T., Mironov, V., Gutowska, A., Roth, E.A., and Markwald, R.R. (2003). Cell and organ printing 2: fusion of cell aggregates in three-dimensional gels. Anat. Rec. A Discov. Mol. Cell. Evol. Biol. *272*, 497–502. https://doi.org/10.1002/ar.a.10059.

6. Schaffner, M., Rühs, P.A., Coulter, F., Kilcher, S., and Studart, A.R. (2017). 3D printing of bacteria into functional complex materials. Sci. Adv. *3*, eaao6804. https://doi.org/10.1126/sciadv.aao6804.

7. Dhariwala, B., Hunt, E., and Boland, T. (2004). Rapid prototyping of tissue-engineering constructs, using photopolymerizable hydrogels and stereolithography. Tissue Eng. *10*, 1316–1322.

8. Peak, C.W., Stein, J., Gold, K.A., and Gaharwar, A.K. (2018). Nanoengineered colloidal inks for 3D bioprinting. Langmuir *34*, 917–925.

9. Hull, S.M., Brunel, L.G., and Heilshorn, S.C. (2022). 3D bioprinting of cell-laden hydrogels for improved biological functionality. Adv. Mater. *34*, e2103691. https://doi.org/10.1002/adma.202103691.

10. Lee, J.M., Ng, W.L., and Yeong, W.Y. (2019). Resolution and shape in bioprinting: strategizing towards complex tissue and organ printing. Appl. Phys. Rev. *6*, 011307.

11. Lee, J.M., and Yeong, W.Y. (2016). Design and printing strategies in 3D bioprinting of cell-hydrogels: areview. Adv. Healthc. Mater. *5*, 2856–2865. https://doi.org/10.1002/adhm.201600435.

12. Li, J., Chen, M., Fan, X., and Zhou, H. (2016). Recent advances in bioprinting techniques: approaches, applications and future prospects. J. Transl. Med. *14*, 271.

13. Huang, Y., Zhang, X.F., Gao, G., Yonezawa, T., and Cui, X. (2017). 3D bioprinting and the current applications in tissue engineering. Biotechnol. J. *12*, 1600734.

14. Melchels, F.P.W., Feijen, J., and Grijpma, D.W. (2010). A review on stereolithography and its applications in biomedical engineering. Biomaterials *31*, 6121–6130.

15. Sears, N.A., Seshadri, D.R., Dhavalikar, P.S., and Cosgriff-Hernandez, E. (2016). A review of three-dimensional printing in tissue engineering. Tissue Eng. Part B Rev. *22*, 298–310. https://doi.org/10.1089/ten.TEB.2015.0464.

16. Pagac, M., Hajnys, J., Ma, Q.P., Jancar, L., Jansa, J., Stefek, P., and Mesicek, J. (2021). A review of vat photopolymerization technology: materials, applications, challenges, and future trends of 3D printing. Polymers *13*, 598. https://doi.org/10.3390/polym13040598.

17. Gu, B.K., Choi, D.J., Park, S.J., Kim, M.S., Kang, C.M., and Kim, C.H. (2016). 3-dimensional bioprinting for tissue engineering applications. Biomater. Res. *20*, 12. https://doi.org/10.1186/s40824-016-0058-2.

18. Li, W., Mille, L.S., Robledo, J.A., Uribe, T., Huerta, V., and Zhang, Y.S. (2020). Recent advances in formulating and processing biomaterial inks for vat polymerization-based 3D printing. Adv. Healthc. Mater. *9*, e2000156. https://doi.org/10.1002/adhm.202000156.

19. Hölzl, K., Lin, S., Tytgat, L., Van Vlierberghe, S., Gu, L., and Ovsianikov, A. (2016). Bioink properties before, during and after 3D bioprinting. Biofabrication *8*, 032002.

20. Gopinathan, J., and Noh, I. (2018). Recent trends in bioinks for 3D printing. Biomater. Res. *22*, 11. https://doi.org/10.1186/s40824-018-0122-1.

21. Ji, S., and Guvendiren, M. (2017). Recent advances in bioink design for 3D bioprinting of tissues and organs. Front. Bioeng. Biotechnol. *5*, 23. https://doi.org/10.3389/fbioe.2017.00023.

22. Calvert, P., and Zengshe, L. (1998). Freeform fabrication of hydrogels. Acta Mater. *46*, 2565–2571.

23. Bártolo, P.J. (2011). Stereolithography: Materials, Processes and Applications (Springer Science & Business Media).

24. Manapat, J.Z., Chen, Q., Ye, P., and Advincula, R.C. (2017). 3D printing of polymer nanocomposites via stereolithography. Macromol. Mater. Eng. *302*, 1600553.

25. Ngo, T.D., Kashani, A., Imbalzano, G., Nguyen, K.T., and Hui, D. (2018). Additive manufacturing (3D printing): a review of materials, methods, applications and challenges. Compos. B Eng. *143*, 172–196.

26. Schmidleithner, C., and Kalaskar, D.M. (2018). Stereolithography. In IntechOpen.

27. Wang, J., Goyanes, A., Gaisford, S., and Basit, A.W. (2016). Stereolithographic (SLA) 3D printing of oral modified-release dosage forms. Int. J. Pharm. *503*, 207–212. https://doi.org/10.1016/j.ijpharm.2016.03.016.

28. Stampfl, J., Baudis, S., Heller, C., Liska, R., Neumeister, A., Kling, R., Ostendorf, A., and Spitzbart, M. (2008). Photopolymers with tunable mechanical properties processed by laser-based high-resolution stereolithography. J. Micromech. Microeng. *18*, 125014.

29. Arcaute, K., Mann, B.K., and Wicker, R.B. (2006). Stereolithography of three-dimensional bioactive poly (ethylene glycol) constructs with encapsulated cells. Ann. Biomed. Eng. *34*, 1429–1441.

30. Chan, V., Zorlutuna, P., Jeong, J.H., Kong, H., and Bashir, R. (2010). Three-dimensional photopatterning of hydrogels using stereolithography for long-term cell encapsulation. Lab Chip *10*, 2062–2070.

31. Mouzakis, D.E. (2018). Advanced technologies in manufacturing 3D-layered structures for defense and aerospace. LaminationTheory Appl. 89–113.

32. Ng, W.L., Lee, J.M., Zhou, M., Chen, Y.-W., Lee, K.-X.A., Yeong, W.Y., and Shen, Y.-F. (2020). Vat polymerization-based bioprinting—process, materials, applications and regulatory challenges. Biofabrication *12*, 022001.

33. Li, W., Wang, M., Mille, L.S., Robledo Lara, J.A., Huerta, V., Uribe Velázquez, T., Cheng, F., Li, H., Gong, J., Ching, T., et al. (2021). A smartphone-enabled portable digital light processing 3D printer. Adv. Mater. *33*, 2102153.

34. Mondschein, R.J., Kanitkar, A., Williams, C.B., Verbridge, S.S., and Long, T.E. (2017). Polymer structure-property requirements for stereolithographic 3D printing of soft tissue engineering scaffolds. Biomaterials *140*, 170–188.

35. Han, L.-H., Mapili, G., Chen, S., and Roy, K. (2008). Projection microfabrication of three-dimensional scaffolds for tissue engineering. J. Manuf. Sci. Eng. *130*.

36. Pan, Y., Zhou, C., and Chen, Y. (2012). A fast mask projection stereolithography process for fabricating digital models in minutes. J. Manuf. Sci. Eng. *134*.

37. Zhang, A.P., Qu, X., Soman, P., Hribar, K.C., Lee, J.W., Chen, S., and He, S. (2012). Rapid fabrication of complex 3D extracellular microenvironments by dynamic optical projection stereolithography. Adv. Mater. *24*, 4266–4270. https://doi.org/10.1002/adma.201202024.

38. Kumar, H., and Kim, K. (2020). Stereolithography 3D bioprinting. In 3D Bioprinting (Springer), pp. 93–108.

39. Zhu, W., Ma, X., Gou, M., Mei, D., Zhang, K., and Chen, S. (2016). 3D printing of functional biomaterials for tissue engineering. Curr. Opin. Biotechnol. *40*, 103–112. https://doi.org/10.1016/j.copbio.2016.03.014.

40. Doraiswamy, A., Narayan, R.J., Harris, M.L., Qadri, S.B., Modi, R., and Chrisey, D.B. (2007). Laser microfabrication of hydroxyapatite-osteoblast-like cell composites. J. Biomed. Mater. Res. *80*, 635–643. https://doi.org/10.1002/jbm.a.30969.

41. Schwartz, J.J., and Boydston, A.J. (2019). Multimaterial actinic spatial control 3D and 4D printing. Nat. Commun. *10*, 791. https://doi.org/10.1038/s41467-019-08639-7.

42. Grigoryan, B., Paulsen, S.J., Corbett, D.C., Sazer, D.W., Fortin, C.L., Zaita, A.J., Greenfield, P.T., Calafat, N.J., Gounley, J.P., Ta, A.H., et al. (2019). Multivascular networks and functional intravascular topologies within biocompatible hydrogels. Science *364*, 458–464. https://doi.org/10.1126/science.aav9750.

43. Schweiger, J., Edelhoff, D., and Güth, J.F. (2021). 3D printing in digital prosthetic dentistry: an overview of recent developments in additive manufacturing. J. Clin. Med. *10*, 2010.

44. Kellermann, K.I., and Moran, J.M. (2001). The development of high-resolution imaging in radio astronomy. Annu. Rev. Astron. Astrophys. *39*, 457–509.

45. Bagheri, A., and Jin, J. (2019). Photopolymerization in 3D printing. ACS Appl. Polym. Mater. *1*, 593–611.

46. Krishnamoorthy, S., Wadnap, S., Noorani, B., Xu, H., and Xu, C. (2020). Investigation of

gelatin methacrylate working curves in dynamic optical projection stereolithography of vascular-like constructs. Eur. Polym. J. *124*, 109487.

47. Wang, Z., Abdulla, R., Parker, B., Samanipour, R., Ghosh, S., and Kim, K. (2015). A simple and high-resolution stereolithography-based 3D bioprinting system using visible light crosslinkable bioinks. Biofabrication *7*, 045009.

48. Yang, K.-H., Lindberg, G., Soliman, B., Lim, K., Woodfield, T., and Narayan, R.J. (2021). Effect of photoinitiator on precursory stability and curing depth of Thiol-Ene Clickable gelatin. Polymers *13*, 1877.

49. Kim, H., Kang, B., Cui, X., Lee, S., Lee, K., Cho, D., Hwang, W., Woodfield, T.B.F., Lim, K.S., and Jang, J. (2021). Light-activated decellularized extracellular matrix-based bioinks for volumetric tissue analogs at the centimeter scale. Adv. Funct. Mater. *31*, 2011252.

50. Castilho, M., Levato, R., Bernal, P.N., de Ruijter, M., Sheng, C.Y., van Duijn, J., Piluso, S., Ito, K., and Malda, J. (2021). Hydrogel-based bioinks for cell electrowriting of well-organized living structures with micrometer-scale resolution. Biomacromolecules *22*, 855–866. https://doi.org/10.1021/acs.biomac.0c01577.

51. Yu, C., Schimelman, J., Wang, P., Miller, K.L., Ma, X., You, S., Guan, J., Sun, B., Zhu, W., and Chen, S. (2020). Photopolymerizable biomaterials and light-based 3D printing strategies for biomedical applications. Chem. Rev. *120*, 10695–10743. https://doi.org/10.1021/acs.chemrev.9b00810.

52. Zhang, J., Hu, Q., Wang, S., Tao, J., and Gou, M. (2020). Digital light processing based three-dimensional printing for medical applications. Int. J. Bioprint. *6*, 242. https://doi.org/10.18063/ijb.v6i1.242.

53. Trachtenberg, J.E., Santoro, M., Williams, C., III, Piard, C.M., Smith, B.T., Placone, J.K., Menegaz, B.A., Molina, E.R., Lamhamedi-Cherradi, S.-E., Ludwig, J.A., et al. (2018). Effects of shear stress gradients on ewing sarcoma cells using 3D printed scaffolds and flow perfusion. ACS Biomater. Sci. Eng. *4*, 347–356.

54. Li, Y., Mao, Q., Li, X., Yin, J., Wang, Y., Fu, J., and Huang, Y. (2019). High-fidelity and high-efficiency additive manufacturing using tunable pre-curing digital light processing. Addit. Manuf. *30*, 100889.

55. Zhang, R., and Larsen, N.B. (2017). Stereolithographic hydrogel printing of 3D culture chips with biofunctionalized complex 3D perfusion networks. Lab Chip *17*, 4273–4282.

56. Lim, K.S., Galarraga, J.H., Cui, X., Lindberg, G.C.J., Burdick, J.A., and Woodfield, T.B.F. (2020). Fundamentals and applications of photo-cross-linking in bioprinting. Chem. Rev. *120*, 10662–10694. https://doi.org/10.1021/acs.chemrev.9b00812.

57. Beh, C.W., Yew, D.S., Chai, R.J., Chin, S.Y., Seow, Y., and Hoon, S.S. (2021). A fluid-supported 3D hydrogel bioprinting method. Biomaterials *276*, 121034. https://doi.org/10.1016/j.biomaterials.2021.121034.

58. Sun, Y., Yu, K., Nie, J., Sun, M., Fu, J., Wang, H., and He, Y. (2021). Modeling the printability of photocuring and strength adjustable hydrogel bioink during projection-based 3D bioprinting. Biofabrication *13*, 035032. https://doi.org/10.1088/1758-5090/aba413.

59. Wang, M., Li, W., Hao, J., Gonzales, A., 3rd, Zhao, Z., Flores, R.S., Kuang, X., Mu, X., Ching, T., Tang, G., et al. (2022). Molecularly cleavable bioinks facilitate high-performance digital light processing-based bioprinting of functional volumetric soft tissues. Nat. Commun. *13*, 3317. https://doi.org/10.1038/s41467-022-31002-2.

60. Keane, T.J., and Badylak, S.F. (2014). In Biomaterials for Tissue Engineering Applications, *3*Biomaterials for Tissue Engineering Applications (Elsevier), pp. 112–118.

61. Yue, K., Trujillo-de Santiago, G., Alvarez, M.M., Tamayol, A., Annabi, N., and Khademhosseini, A. (2015). Synthesis, properties, and biomedical applications of gelatin methacryloyl (GelMA) hydrogels. Biomaterials *73*, 254–271. https://doi.org/10.1016/j.biomaterials.2015.08.045.

62. Nichol, J.W., Koshy, S.T., Bae, H., Hwang, C.M., Yamanlar, S., and Khademhosseini, A. (2010). Cell-laden microengineered gelatin methacrylate hydrogels. Biomaterials *31*, 5536–5544. https://doi.org/10.1016/j.biomaterials.2010.03.064.

63. Ying, G., Jiang, N., Yu, C., and Zhang, Y.S. (2018). Three-dimensional bioprinting of gelatin methacryloyl (GelMA). Biodes. Manuf. *1*, 215–224.

64. Ma, X., Qu, X., Zhu, W., Li, Y.-S., Yuan, S., Zhang, H., Liu, J., Wang, P., Lai, C.S.E., Zanella, F., et al. (2016). Deterministically patterned biomimetic human iPSC-derived hepatic model via rapid 3D bioprinting. Proc. Natl. Acad. Sci. USA *113*, 2206–2211.

65. Wang, Z., Kumar, H., Tian, Z., Jin, X., Holzman, J.F., Menard, F., and Kim, K. (2018). Visible light photoinitiation of cell-adhesive gelatin methacryloyl hydrogels for stereolithography 3D bioprinting. ACS Appl. Mater. Interfaces *10*, 26859–26869.

66. Bertlein, S., Brown, G., Lim, K.S., Jungst, T., Boeck, T., Blunk, T., Tessmar, J., Hooper, G.J., Woodfield, T.B.F., and Groll, J. (2017). Thiol-ene clickable gelatin: aplatform bioink for multiple 3D biofabrication technologies. Adv. Mater. *29*, 1703404. https://doi.org/10.1002/adma.201703404.

67. Ma, X., Yu, C., Wang, P., Xu, W., Wan, X., Lai, C.S.E., Liu, J., Koroleva-Maharajh, A., and Chen, S. (2018). Rapid 3D bioprinting of decellularized extracellular matrix with regionally varied mechanical properties and biomimetic microarchitecture. Biomaterials *185*, 310–321. https://doi.org/10.1016/j.biomaterials.2018.09.026.

68. Yu, C., Ma, X., Zhu, W., Wang, P., Miller, K.L., Stupin, J., Koroleva-Maharajh, A., Hairabedian, A., and Chen, S. (2019). Scanningless and continuous 3D bioprinting of human tissues with decellularized extracellular matrix. Biomaterials *194*, 1–13. https://doi.org/10.1016/j.biomaterials.2018.12.009.

69. Kim, S.H., Yeon, Y.K., Lee, J.M., Chao, J.R., Lee, Y.J., Seo, Y.B., Sultan, M.T., Lee, O.J., Lee, J.S., Yoon, S.I., et al. (2018). Precisely printable and biocompatible silk fibroin bioink for digital light processing 3D printing. Nat. Commun. *9*, 1620. https://doi.org/10.1038/s41467-018-03759-y.

70. Wang, X., Ao, Q., Tian, X., Fan, J., Tong, H., Hou, W., and Bai, S. (2017). Gelatin-based hydrogels for organ 3D bioprinting. Polymers *9*, 401. https://doi.org/10.3390/polym9090401.

71. Yoon, H.J., Shin, S.R., Cha, J.M., Lee, S.H., Kim, J.H., Do, J.T., Song, H., and Bae, H. (2016). Cold water fish gelatin methacryloyl hydrogel for tissue engineering application. PLoS One *11*, e0163902. https://doi.org/10.1371/journal.pone.0163902.

72. Wang, M., Li, W., Luo, Z., Tang, G., Mu, X., Kuang, X., Guo, J., Zhao, Z., Flores, R.S., Jiang, Z., et al. (2022). A multifunctional micropore-forming bioink with enhanced anti-bacterial and anti-inflammatory properties. Biofabrication *14*, 024105. https://doi.org/10.1088/1758-5090/ac5936.

73. Levato, R., Lim, K.S., Li, W., Asua, A.U., Peña, L.B., Wang, M., Falandt, M., Bernal, P.N., Gawlitta, D., Zhang, Y.S., et al. (2021). High-resolution lithographic biofabrication of hydrogels with complex microchannels from low-temperature-soluble gelatin bioresins. Mater. Today. Bio *12*, 100162. https://doi.org/10.1016/j.mtbio.2021.100162.

74. García-Lizarribar, A., Fernández-Garibay, X., Velasco-Mallorquí, F., Castaño, A.G., Samitier, J., and Ramon-Azcon, J. (2018). Composite biomaterials as long-lasting scaffolds for 3D bioprinting of highly aligned muscle tissue. Macromol. Biosci. *18*, 1800167.

75. Hoyle, C.E., and Bowman, C.N. (2010). Thiol-ene click chemistry. Angew. Chem. Int. Ed. Engl. *49*, 1540–1573. https://doi.org/10.1002/anie.200903924.

76. Ahangarpour, M., Kavianinia, I., Harris, P.W.R., and Brimble, M.A. (2021). Photo-induced radical thiol-ene chemistry: a versatile toolbox for peptide-based drug design. Chem. Soc. Rev. *50*, 898–944. https://doi.org/10.1039/d0cs00354a.

77. Frischknecht, R., and Seidenbecher, C.I. (2008). The crosstalk of hyaluronan-based extracellular matrix and synapses. Neuron Glia Biol. *4*, 249–257. https://doi.org/10.1017/S1740925X09990226.

78. Bencherif, S.A., Srinivasan, A., Horkay, F., Hollinger, J.O., Matyjaszewski, K., and Washburn, N.R. (2008). Influence of the degree of methacrylation on hyaluronic acid hydrogels properties. Biomaterials *29*,

1739–1749. https://doi.org/10.1016/j.biomaterials.2007.11.047.

79. Noh, I., Kim, N., Tran, H.N., Lee, J., and Lee, C. (2019). 3D printable hyaluronic acid-based hydrogel for its potential application as a bioink in tissue engineering. Biomater. Res. *23*, 3.

80. Lam, T., Dehne, T., Krüger, J.P., Hondke, S., Endres, M., Thomas, A., Lauster, R., Sittinger, M., and Kloke, L. (2019). Photopolymerizable gelatin and hyaluronic acid for stereolithographic 3D bioprinting of tissue-engineered cartilage. J. Biomed. Mater. Res. B Appl. Biomater. *107*, 2649–2657. https://doi.org/10.1002/jbm.b.34354.

81. Frantz, C., Stewart, K.M., and Weaver, V.M. (2010). The extracellular matrix at a glance. J. Cell Sci. *123*, 4195–4200.

82. Badylak, S.F. (2007). The extracellular matrix as a biologic scaffold material. Biomaterials *28*, 3587–3593.

83. Smoak, M.M., Hogan, K.J., Grande-Allen, K.J., and Mikos, A.G. (2021). Bioinspired electrospun dECM scaffolds guide cell growth and control the formation of myotubes. Sci. Adv. *7*, eabg4123. https://doi.org/10.1126/sciadv.abg4123.

84. Pati, F., Jang, J., Ha, D.H., Won Kim, S., Rhie, J.W., Shim, J.H., Kim, D.H., and Cho, D.W. (2014). Printing three-dimensional tissue analogues with decellularized extracellular matrix bioink. Nat. Commun. *5*, 3935. https://doi.org/10.1038/ncomms4935.

85. Kasoju, N., and Bora, U. (2012). Silk fibroin in tissue engineering. Adv. Healthc. Mater. *1*, 393–412.

86. Dey, S., Jaiswal, C., Shome, S., Bhar, B., Bandyopadhyay, A., Manikumar, K., Dadheech, R., and Mandal, B.B. (2022). Photocrosslinkable silk-based biomaterials for regenerative medicine and healthcare applications. Regen. Eng. Transl. Med. 1–21.

87. Chattopadhyay, S., and Raines, R.T. (2014). Review collagen-based biomaterials for wound healing. Biopolymers *101*, 821–833. https://doi.org/10.1002/bip.22486.

88. Drzewiecki, K.E., Malavade, J.N., Ahmed, I., Lowe, C.J., and Shreiber, D.I. (2017). A thermoreversible, photocrosslinkable collagen bio-ink for free-form fabrication of scaffolds for regenerative medicine. Technology (Singap World Sci) *5*, 185–195. https://doi.org/10.1142/S2339547817500091.

89. Axpe, E., and Oyen, M.L. (2016). Applications of alginate-based bioinks in 3D bioprinting. Int. J. Mol. Sci. *17*, 1976. https://doi.org/10.3390/ijms17121976.

90. Jeon, O., Bouhadir, K.H., Mansour, J.M., and Alsberg, E. (2009). Photocrosslinked alginate hydrogels with tunable biodegradation rates and mechanical properties. Biomaterials *30*, 2724–2734. https://doi.org/10.1016/j.biomaterials.2009.01.034.

91. Ahmadi, F., Oveisi, Z., Samani, S.M., and Amoozgar, Z. (2015). Chitosan based hydrogels: characteristics and pharmaceutical applications. Res. Pharm. Sci. *10*, 1–16.

92. Akopova, T.A., Demina, T.S., Cherkaev, G.V., Khavpachev, M.A., Bardakova, K.N., Grachev, A.V., Vladimirov, L.V., Zelenetskii, A.N., and Timashev, P.S. (2019). Solvent-free synthesis and characterization of allyl chitosan derivatives. RSC Adv. *9*, 20968–20975.

93. Lee, M., Rizzo, R., Surman, F., and Zenobi-Wong, M. (2020). Guiding lights: tissue bioprinting using photoactivated materials. Chem. Rev. *120*, 10950–11027.

94. Zhu, J., Beamish, J.A., Tang, C., Kottke-Marchant, K., and Marchant, R.E. (2006). Extracellular matrix-like cell-adhesive hydrogels from RGD-containing poly (ethylene glycol) diacrylate. Macromolecules *39*, 1305–1307.

95. Wang, M., Li, W., Tang, G., Garciamendez-Mijares, C.E., and Zhang, Y.S. (2021). Engineering (bio) materials through shrinkage and expansion. Adv. Healthc. Mater. *10*, 2100380.

96. Koffler, J., Zhu, W., Qu, X., Platoshyn, O., Dulin, J.N., Brock, J., Graham, L., Lu, P., Sakamoto, J., Marsala, M., et al. (2019). Biomimetic 3D-printed scaffolds for spinal cord injury repair. Nat. Med. *25*, 263–269. https://doi.org/10.1038/s41591-018-0296-z.

97. Lim, K.S., Levato, R., Costa, P.F., Castilho, M.D., Alcala-Orozco, C.R., van Dorenmalen, K.M.A., Melchels, F.P.W., Gawlitta, D., Hooper, G.J., Malda, J., and Woodfield, T.B.F. (2018). Bio-resin for high resolution lithography-based biofabrication of complex cell-laden constructs. Biofabrication *10*, 034101. https://doi.org/10.1088/1758-5090/aac00c.

98. Singh, D., Harding, A.J., Albadawi, E., Boissonade, F.M., Haycock, J.W., and Claeyssens, F. (2018). Additive manufactured biodegradable poly(glycerol sebacate methacrylate) nerve guidance conduits. Acta Biomater. *78*, 48–63. https://doi.org/10.1016/j.actbio.2018.07.055.

99. Wang, M., Zhou, Y., Shi, D., Chang, R., Zhang, J., Keidar, M., and Webster, T.J. (2019). Cold atmospheric plasma (CAP)-modified and bioactive protein-loaded core-shell nanofibers for bone tissue engineering applications. Biomater. Sci. *7*, 2430–2439. https://doi.org/10.1039/c8bm01284a.

100. Rai, R., Tallawi, M., Grigore, A., and Boccaccini, A.R. (2012). Synthesis, properties and biomedical applications of poly (glycerol sebacate)(PGS): a review. Prog. Polym. Sci. *37*, 1051–1078.

101. Vogt, L., Ruther, F., Salehi, S., and Boccaccini, A.R. (2021). Poly(Glycerol sebacate) in biomedical applications-A review of the recent literature. Adv. Healthc. Mater. *10*, e2002026. https://doi.org/10.1002/adhm.202002026.

102. Motlagh, D., Yang, J., Lui, K.Y., Webb, A.R., and Ameer, G.A. (2006). Hemocompatibility evaluation of poly(glycerol-sebacate) in vitro for vascular tissue engineering. Biomaterials *27*, 4315–4324. https://doi.org/10.1016/j.biomaterials.2006.04.010.

103. Raman, R., and Bashir, R. (2015). Stereolithographic 3D bioprinting for biomedical applications. Essentials 3D Biofabrication Translat. 89–121. https://doi.org/10.1016/B978-0-12-800972-7.00006-2.

104. Wang, C., Tang, Z., Zhao, Y., Yao, R., Li, L., and Sun, W. (2014). Three-dimensional in vitro cancer models: a short review. Biofabrication *6*, 022001. https://doi.org/10.1088/1758-5082/6/2/022001.

105. Samavedi, S., and Joy, N. (2017). 3D printing for the development of in vitro cancer models. Curr. Opin. Biomed. Eng. *2*, 35–42.

106. Zorlutuna, P., Jeong, J.H., Kong, H., and Bashir, R. (2011). Stereolithography-based hydrogel microenvironments to examine cellular interactions. Adv. Funct. Mater. *21*, 3642–3651. https://doi.org/10.1002/adfm.201101023.

107. Zhou, X., Zhu, W., Nowicki, M., Miao, S., Cui, H., Holmes, B., Glazer, R.I., and Zhang, L.G. (2016). 3D bioprinting a cell-laden bone matrix for breast cancer metastasis study. ACS Appl. Mater. Interfaces *8*, 30017–30026. https://doi.org/10.1021/acsami.6b10673.

108. Tang, M., Xie, Q., Gimple, R.C., Zhong, Z., Tam, T., Tian, J., Kidwell, R.L., Wu, Q., Prager, B.C., Qiu, Z., et al. (2020). Three-dimensional bioprinted glioblastoma microenvironments model cellular dependencies and immune interactions. Cell Res. *30*, 833–853. https://doi.org/10.1038/s41422-020-0338-1.

109. Tang, M., Tiwari, S.K., Agrawal, K., Tan, M., Dang, J., Tam, T., Tian, J., Wan, X., Schimelman, J., You, S., et al. (2021). Rapid 3D bioprinting of glioblastoma model mimicking native biophysical heterogeneity. Small *17*, 2006050.

110. Liu, J., Miller, K., Ma, X., Dewan, S., Lawrence, N., Whang, G., Chung, P., McCulloch, A.D., and Chen, S. (2020). Direct 3D bioprinting of cardiac micro-tissues mimicking native myocardium. Biomaterials *256*, 120204. https://doi.org/10.1016/j.biomaterials.2020.120204.

111. Mota, C., Camarero-Espinosa, S., Baker, M.B., Wieringa, P., and Moroni, L. (2020). Bioprinting: from tissue and organ development to in vitro models. Chem. Rev. *120*, 10547–10607. https://doi.org/10.1021/acs.chemrev.9b00789.

112. Jorgensen, A.M., Yoo, J.J., and Atala, A. (2020). Solid organ bioprinting: strategies to achieve organ function. Chem. Rev. *120*, 11093–11127. https://doi.org/10.1021/acs.chemrev.0c00145.

113. Hong, H., Seo, Y.B., Kim, D.Y., Lee, J.S., Lee, Y.J., Lee, H., Ajiteru, O., Sultan, M.T., Lee, O.J., Kim, S.H., and Park, C.H. (2020). Digital

light processing 3D printed silk fibroin hydrogel for cartilage tissue engineering. Biomaterials *232*, 119679. https://doi.org/10.1016/j.biomaterials.2019.119679.

114. Zhu, W., Qu, X., Zhu, J., Ma, X., Patel, S., Liu, J., Wang, P., Lai, C.S.E., Gou, M., Xu, Y., et al. (2017). Direct 3D bioprinting of prevascularized tissue constructs with complex microarchitecture. Biomaterials *124*, 106–115. https://doi.org/10.1016/j.biomaterials.2017.01.042.

115. Peng, X., Kuang, X., Roach, D.J., Wang, Y., Hamel, C.M., Lu, C., and Qi, H.J. (2021). Integrating digital light processing with direct ink writing for hybrid 3D printing of functional structures and devices. Addit. Manuf. *40*, 101911.

116. Hwang, H.H., You, S., Ma, X., Kwe, L., Victorine, G., Lawrence, N., Wan, X., Shen, H., Zhu, W., and Chen, S. (2021). High throughput direct 3D bioprinting in multiwell plates. Biofabrication *13*, 025007.

117. Miller, K.L., Xiang, Y., Yu, C., Pustelnik, J., Wu, J., Ma, X., Matsui, T., Imahashi, K., and Chen, S. (2021). Rapid 3D BioPrinting of a human iPSC-derived cardiac micro-tissue for high-throughput drug testing. Organs-on-a-Chip *3*, 100007.

118. Chen, Y., Zhang, J., Liu, X., Wang, S., Tao, J., Huang, Y., Wu, W., Li, Y., Zhou, K., Wei, X., et al. (2020). Noninvasive in vivo 3D bioprinting. Sci. Adv. *6*, eaba7406. https://doi.org/10.1126/sciadv.aba7406.